Norwegian University
of Life Sciences

Master's Thesis 2020 30 ECTS
Faculty of Science and Technology

Power Prediction and Wake Losses in Offshore Wind Farms with the Dynamic Wake Meandering Model

John Sondre Sikkeland
MSc. Environmental Physics and Renewable Energy

Acknowlegdements

First of all, my deepest gratitude goes to my supervisors Tor Anders Nygaard and Øyvind Waage Hanssen-Bauer from IFE. Their help and guidance has been very important for shaping this thesis, by answering questions and providing constructive and supportive feedback. Furthermore, I also thank Jacobus de Vaal from IFE, who together with Øyvind has clarified questions about the code. Further, I thank Gunner Chr. Larsen for suggesting the topic for this thesis. My appretiation also goes to Ingemar Carlén from Teknikgruppen, who has provided essential guidance for the dataset, and clarifying questions about this. I would also thank Anders Sommer from Vattenfall and Peder Enevoldsen from Siemens Gamesa, who has provided the dataset used in this thesis. Furthermore, I would thank Rolf-Erik Keck for clarifying questions regarding his thesis and DWM model.

At last, I thank my family and friends for the love and support throughout all these years. A particular appreciation goes to my fellow students studying Environmental Physics and Renewable Energy. These five years at the university would not have been the same without you.

Ås, Aug 17th 2020

John Sondre Sikkeland

Summary

The global wind energy production is increasing, and wind energy is expected to be one of the dominating energy sources for generation of electricity in a couple of decades. To achieve this, wind farms are built as big clusters of wind turbines. The wind conditions inside these farms are different compared to the free-stream conditions, and the area behind the upstream turbines is known as the wake. Turbines operating in the wake of other turbines are experiencing higher loads and reduced power production. As a consequence of this, accurate engineering models are needed to predict the loads and power production for the turbines in wind farms.

For this purpose, the Dynamic Wake Meandering model was developed several years ago. Previous studies have shown that the model predicts loads and power production in wind farms with high accuracy for wind speeds below the rated wind speed of the turbine. However, the model fails around rated wind speed, and particularly power production above rated wind speed has not been thoroughly investigated with the model. As a consequence of this, the main goal of this thesis is to investigate the power production around rated wind speed and above rated wind speed.

For this purpose, three different methods for treating wake merging are used to predict the wake losses over a wide range of wind speeds. The first method is based on a dominant wake approach, while the two other methods do linear and squared summation of the velocity deficits in the wakes. The performance of these methods are validated against full-scale field data from Lillgrund, an offshore wind farm located outside the southwest coast of Sweden. The results show that the first method has a fine agreement with the field data well below rated wind speed, where it overestimates the power production with 6% at 10 m/s, but fails for wind speeds exceeding 10 m/s. The method based on linear summation is better than the two the other above rated wind speed. A problem with the model is the fact that the model overpredicts the wake losses for most of the wind speeds above 10 m/s already at turbine 2, which reduces the validity of the wake merging methods.

The conclusion is that the model is a nice tool for predicting the power production and wake losses in offshore wind parks below and above rated wind speed, but fails around rated wind speed. To improve this, it is important to model the wake loss behind the first turbine in the row accurately, for better validation of the wake merging methods around rated wind speed. Moreover, the wake merging procedure could also be improved. This could be achieved by introducing new methods for wake merging, or by testing other existing summation methods. Furthermore, a

even more consistent formulation of the turbulence build-up might improve ability of the Dynamic Wake Meandering model to estimate wake losses over a wide range of wind speeds.

Sammendrag

Den globale produksjonen av vindenergi er økende, og vindenergi er forventet å være en de dominerende energikildene for produksjon av elektrisitet om et par tiår. For å oppnå dette blir flere og flere vindparker bygget, bestående av store samlinger med vindturbiner. Vindforholdene innenfor disse parkene er annerledes enn forholdene utenfor, og området bak en oppstrøms turbin kalles vake. Turbiner som operer i vaken til andre turbiner kjennetegnes ved at de opplever høyere laster og redusert effektproduksjon. Som en konsekvens av dette, er det nødvendig med presise modeller til å predikere laster og effektproduksjon for tubiner i vindparker.

For dette formålet ble "Dynamic Wake Meandering" modellen utviklet for flere år siden. Tidligere studier har vist at modellen predikerer laster og effektproduksjon i vindparker med høy presisjon for vindhastiheter under tubinens nominelle vindhastighet. Det er samtidig vist at modellen feiler rundt nominell vindhastighet, og effektproduksjonen over nominell vindhastighet har ikke blitt undersøkt nøye med modellen. Som en konsekvens at dette, er hovedformålet med oppgaven å undersøke effektproduksjonen rundt nominell og over nominell vindhastighet.

Til dette formålet er tre forskjellige metoder for summering av vaker benyttet til å predikere vaketapene. Den første metoden er basert på en tilnærming der den tar utgangspunkt i den dominerende vaken. Den andre er basert på en lineær summering av vakene, og den siste er basert på en kvadrert summering av vakene. Ytelsen for disse metodene er validert mot fullskala feltdata data fra Lillgrund vindpark, en havbasert vindpark utenfor sørvest kysten av Sverige. Disse resultatene viser at den første metoden stemmer fint overens med feltdataene godt under nominell vindhastighet, der der den overestimerer effektproduksjonen med 6%, men feiler når vindhastigheten overstiger 10 m/s. Metoden basert på lineær summering er bedre egnet enn de to andre over nominell vindhastighet, som stemmer godt med IEC standaren. Ingen av metodene fungerer ved nominell vindhastighet, men det skyldes delvis at modellen underestimerer vaketapene før summeringen av vakene har begynt.

Konklusjonen er at modellen er et nyttig verktøy for å predikere effektproduksjonen i offshore vindparker under og over nominell vindhastighet, men feiler rundt nominell vindhastighet. For å forbedre modellen rundt nominell vindhastighet må vaketapet etter den første turbinen i raden beregnes mer presist, før summeringen av vakene begynner. Da vil metodene for summering av vaker benyttet i denne oppgaven også estimere vaketapene med høyere treffsikkerhet. Videre kan summeringen av vakene potensielt forbedres ved å introdusere nye metoder for summering av vaker, eller å teste andre allerede eksisterende metoder for summer-

ing av vaker. Videre, en mer presis formulering for oppbygning av turbulensen kan potensielt forbedre "Dynamic Wake Meandering" modellens evne til å estimere vaketap for et bredt spekter av vindhastigheter.

Contents

List of Figures

List of Tables

Abbreviations

Abbreviation	Meaning
ABL	Atmospheric Boundary Layer
AC	Aerodynamic Center
CFD	Computational Fluid Dynamics
D	Diameter
DWM	Dynamic Wake Meandering
FFoR	Fixed Frame of Reference
HAWT	Horizontal Axis Wind Turbine
MFoR	Meandering Frame of Reference
LCoE	Levelized Cost of Energy
LE	Leading Edge
LES	Large-Eddy Simulation
TE	Trailing Edge
TI	Turbulence intensity
TSR	Tip Speed Ratio

Nomenclature

Latin symbols	Meaning
A	Rotor area
C_D	Drag coefficient
C_L	Lift coefficient
C_T	Thrust coefficient
C_P	Power coefficient
D	Rotor diameter
D_w	Wake diameter
E	Energy spectrum
F_1	Filter function for ambient turbulence
F_2	Filter function for self-generated turbulence
F_L	Lift force
F_D	Drag force
I_a	Ambient turbulent intensity
L	Monin-Obukhov length
L_u	Length scale in longitudinal direction
N	Number of sequences
N_x	Number of grid points in longitudinal direction
N_y	Number of grid points in lateral direction
N_z	Number of grid points in vertical direction
P	Aerodynamical Power output
P_0	Aerodynamical power of the free-stream wind velocity
P_{max}	Maximum theoretical power output
P_1	Aerodynamical power of the first turbine
R	Rotor radius
R_w	Wake radius
R_{w0}	Wake radius 2D behind rotor
T	Thrust force
T_0	Mean temperature

Latin symbol	Meaning
U	Wind velocity in streamwise direction
U_0	Free-stream wind velocity
U_1	Wind speed of the first turbine
U_d	Centerline velocity deficit
U_d	Centerline velocity deficit 2D behind rotor
U_i	Sequence of the wind speed
U_{mean}	Short-term average longitudinal wind speed
U_r	Velocity at rotor disc
U_{ref}	Velocity in reference height
U_w	Velocity in wake region
a	Axial induction factor
a'	Angular induction factor
c	Chord length
g	Gravitational acceleration
k_1	Calibration factor for ambient turbulence
k_2	Calibration factor for self-generated turbulence
p	Probability
r	Radial coordinate
r_0	Fully expanded radius of rotor disc
t	Time
t	Temporal coordinate
t_0	Time instant
u	Instantaneous longitudinal wind speed
u_*	Friction velocity
v	Instantaneous lateral wind speed
v_c	Large-scale turbulent velocity in lateral direction
w	Instantaneous vertical wind speed
w_c	Large-scale turbulent velocity in vertical direction
x	Axial coordinate and longitudinal coordinate
x_H	Region of the near wake
x_n	Length of near wake
z	Height
z	Vertical coordinate
y	Lateral coordinate
z_0	Roughness length
z_{ref}	Reference height

Combined symbols	Meaning
$\overline{\omega' T'}$	Kinematic virtual heat flux

Greek symbols	Meaning
α	Angle of attach
α	Power exponent
α	Kolmogorov constant
β	Pitch angle
κ	Von Karman constant
λ	Tip speed ratio
μ_T	Eddy viscosity
μ_T^*	Non-dimensional eddy viscosity
ϕ	Inflow angle
ρ	Air density
σ_u	Standard deviation of longitudinal wind speed
Ω	Angular velocity
Ψ	Stability function

Chapter 1

Introduction

1.1 Motivation

Climate change is one of the greatest challenges in the 21st century, where CO_2 from non-renewable energy sources are a major contributor. There has been a growing interest worldwide to increase the renewable energy production, to reduce the emissions of climate gases. Through the Paris agreement in 2015, most of the countries in the world agreed on limiting the global warming with 1.5 degrees, with an absolute maximum limit of 2 degrees [1]. To achieve this, it is extremely important implement more renewable energy in the electricity mix. The EU agreed to a target of 32% renewable energy in the energy demand by 2030. This corresponds to share of 55% renewable energy sources in the electricity generation by 2030 [2].

In 2019, it was installed 60.4 GW of wind power, which is the second best year in the history of the wind industry. Of this, 6.1 GW was offshore wind power, and 2019 is the first year offshore wind has more than 10% of the new installations. This brings the global cumulative wind power capacity up to 651 GW, where offshore wind with an installed capacity of 29 GW reach a total share of 4.5% [3].

The wind turbines installed by the end of 2019 have the potential to cover more than 6% of the global electricity demand [4]. It is expected that the offshore wind power capacity will increase with more than 205 GW by 2030 [5]. By 2050, wind energy is estimated to generate 26% of the global electricity production [6]. Floating offshore wind turbines has a large future potential, but this technology

is not cost-competitive at the moment. By the end of 2019, the global floating offshore wind capacity was 66 MW. It is estimated that 3-19 GW will be built within the next ten years, depending on the development of LCoE [5].

Wind energy has also become one of the most economically beneficially energy sources to implement in the electricity mix, and by 2018, at least 90 countries had commercial wind power installed, where 30 countries had more than 1 GW in operation [7]. In 2019, Europe installed 15.4 GW of new wind power capacity, where 24% of this were offshore installations. This brings the total wind power capacity in Europe to 205 GW. With a generation of 417 TWh in 2019, wind power contributed to 15% of the European electricity demand [8]. The global weighted average LCoE of commissioned onshore wind farm in 2018 was 0.056$/kWh, where a reduction to 0.048 $/kWh by 2020 is estimated. The global weighed average LCoE is 0.127 $/kWh for offshore wind farms, where this is estimated to 0.108 $/kWh in 2022 [9]. For floating offshore wind, the LCoE for pre-commercial projects is in the order of 0.18-0.20 /kWh. This is expected to be reduced to 0.040-0.060 /kWh in 2030 [2]

A great challenge in wind energy production is the variation of the wind, and to predict the power output. The variation in the wind increases fatigue loads on both tower and rotor, and creates a turbulent field downstream of the turbine. The region behind the turbine is called wake. The wind speed in this region is decreased due to the power extracted from the turbine. Turbines located downstream in the wake of other turbine will therefore produce less power than the upstream turbine, and experience greater loads. It is therefore crucial to know how the wake behaves and develops in the downstream region, to predict the power production and the flow characteristics in the wind farm.

1.2 Previous work

Wake losses has been a topic since the beginning of the wind turbine reesarch in the 1970's, where Lissamann [10] was one of the first to address this issue back in 1979, where the terms near and far wake were introduced. A year later, Vermeulen [11] gave an overview of the existing measurements from wind tunnel experiments at the time, and a more detailed description of the near wake and intermediate wake was presented. Ainslie [12] further depeloped the far wake model, implementing the effect of the ambient turbulence as well as the effect of the shear-generated turbulence. The effect of wake meandering was mentioned by Baker and Snel in 1984 [13], and by Ainslie in 1988 [14], but not given much attention otherwise.

The work of Ainslie from 1985 - 1988 inspired the development of the Dynamic Wake meandering (DWM) model. The first version of this model was presented by Madsen et. al [15] in 2003. A detailed description of the fundamental assumptions of the DWM model was presented by Larsen et al. [16], which forms the basis of the newer versions formulated since. A detailed description of the implementation of the model in an aerolastic code was presented by Madsen et al. [17], and fine agreement was obtained by simulating loads in the Egmond Aan Zee wind farm [18]. Moreover, Keck et al. [19] showed a fine agreement for the power losses in the wake. Furthermore, Larsen et al. [20] presented an article in 2015 for load estimation with two different approaches for the wind speed regime above and below rated speed, where the difficulties of predicting loads around rated wind speeds were demonstrated. These two approaches are now implemented in the new IEC standard from 2019 [21].

1.3 Aim of the study

Predicting the power and load regime is of great importance when establishing a wind farm. Accurate models of wakes inside the wind farm is therefore needed to predict the power production and loads, where the loads also affect the life expectancy and the maintenance costs [22].

There has previously been developed several models predicting the wake regime, which started in the late 70s, when the first wind farms were built. However, this has proven to be a difficult task. Most of the previous wake models have simulated the wake losses under rated wind speeds, with good results. The problem rises when the wind speed approaches rated wind speed, and also for wind speeds above this. Although Computational Fluid Dynamics (CFD) and Large Eddy Simulation (LES) have shown promising results, are these models are very computational expensive, with simulation time up to several weeks.

A different method is the DWM model. This model is based on several assumptions, and require significantly less computational time. This model has previously shown promising results for the power and load regime below rated wind speed, but fails above and around rated wind speed. However, the power production around and above rated wind speed has not previously been thoroughly investigated, which leads to an interesting research topic.

The main goal of this study is the following:

- Estimate the power production around rated and above rated wind speed with the DWM model.

The main goal is further divided into the following sub goals:

- Investigate the performance of three different wake merging methods at various wind speeds, and compare them with field measurements.
- Tie the results to already existing theory.
- Identify further improvements for wake merging with the DWM model.

Chapter 2

Theory

2.1 Wind turbine aerodynamics

A wind turbine is a device that converts kinetic energy to mechanical energy. The mechanical energy is further converted to electrical energy by the generator. The most common wind turbine is a three-bladed horizontal axis wind turbine (HAWT). This is the only wind type of wind turbine discussed in this thesis. As the name implies, the rotational axis is horizontal. With the purpose to produce as much energy at an low cost as possible, wind turbines are placed together as clusters in wind farms. The momentum theory and blade element momentum theory described below is covered by Manwell [23], Burton [24] and Hansen [25]

2.1.1 One-dimentional Momentum Theory

It is obviously not possible to extract all of the kinetic energy form the wind, as the wind speed would be reduced to zero in the downstream region of the turbine, and not being able to move away from the turbine. In 1919, the German physicist Albert Betz derived a limit of the maximum amount of energy there is possible to extract from the kinetic energy in the wind. This is based on several simplifying assumptions, such as the turbine is assumed to be an actuator disc, which means infinite number of turbine blades, uniform thrust over the rotor disc, non-rotating wake, steady-state flow, incompressible and inviscious fluid, and constant mass flow along the stream tube.

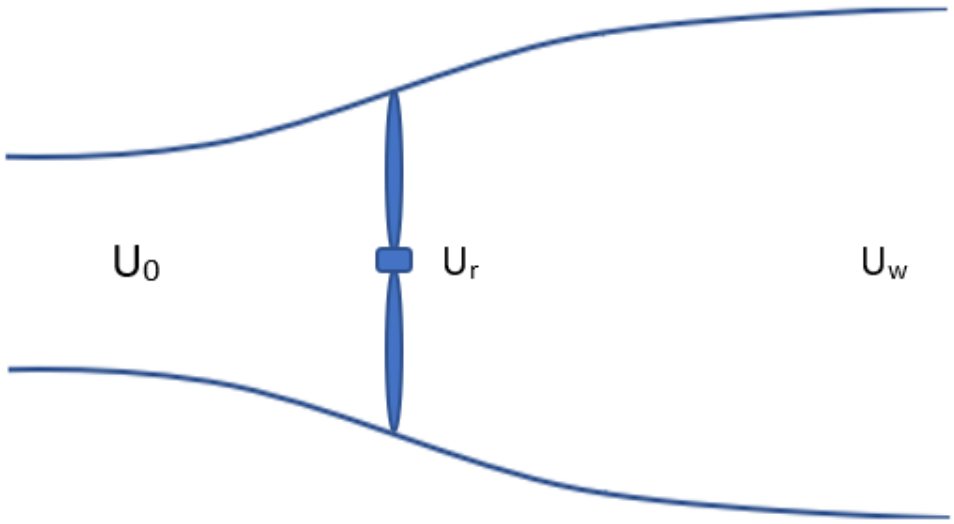

Figure 2.1: Stream tube of a wind turbine. This figure is inspired by Hansen [25]

As the free-stream velocity U_0 approaches the rotor as seen in figure 2.1, the velocity is reduced, and the pressure increases to a level above atmospheric pressure. However, there is a sudden pressure drop right after the wind passes the rotor. As a result of this, the stream tube expands over the rotor, as seen in 2.1. The velocity at the rotor disc is denoted U_r. When the wind passes the rotor, the velocity continues to decrease, until the velocity reaches the wake velocity U_w. At this point, the pressure has recovered to the ambient pressure. The force from the wind in the streamwise direction acting on the rotor is known as the thrust force, resulting from the pressure drop over the rotor. Since an ideal rotor is assumed, the flow is steady-state, frictionless and incrompressible, with no external forces acting on the fluid upstream or downstream of the rotor. Under these assumptions, the Bernoulli equation may be applied, giving the following expression for the thrust force T:

$$T = \frac{1}{2}\rho A(U_0^2 - U_w^2) \tag{2.1}$$

where ρ is the density of the air, and A is area of the rotor. For standard conditions, the density of the air is $1.225\,\mathrm{kg/m^3}$. The axial induction factor a describes the fractional decrease in wind velocity between the free-stream velocity and the velocity at the rotor. An expression for the velocity just behind the rotor is given as:

$$U_r = U_0(1 - a) \tag{2.2}$$

In a similar matter, velocity in the far wake is given by the relation

$$U_w = U_0(1 - 2a) \tag{2.3}$$

From these two equations, it is required that $a < \frac{1}{2}$, otherwise U_w will be less or equal to zero, and the theory will no longer be applicable. The power in the ambient wind , P_0, is found by combining formula for kinetic energy and continuity equation, which gives the formula

$$P_0 = \frac{1}{2}\rho A {U_0}^3 \tag{2.4}$$

The power output P from the wind turbine is found by multiplying the thrust with the velocity at the rotor. The power output P from the turbine is given by the relation

$$P = P_0 C_p \tag{2.5}$$

where the power coefficient C_P is described as:

$$C_P = 4a(1 - a)^2 \tag{2.6}$$

By differentiation of this expression with respect to a and setting the right side of the equation equal to zero, the maximum power coefficient is found to be $C_{p\,max} = \frac{16}{27}$, which approximately equals $C_p = 0.593$, and occurs when $a = \frac{1}{3}$. This is known as the Betz limit. In practice today, wind turbines may reach a power coefficient of $C_P = 0.5$ at optimal wind speed [25].

The thrust force may also be expressed by the thrust coefficient C_T, where C_T is expressed as

$$C_T = 4a(1 - a) \tag{2.7}$$

The thrust force is thus given by the expression

$$T = \frac{1}{2}\rho A U_0^2 C_T \tag{2.8}$$

Power curves and thrust curves that shows the power, power coefficient and thrust coefficient as a function of wind speed are important tools for modelling purposes in the wind industry, and is further explained in chapter 3. Moreover, according to Barthelmie et al. [26], Sanderse [27] and Elliot [28], the largest wake losses occur at wind speeds below rated with high thrust coefficient. It is also stated by Barthelmie et al. [26] that the wake losses are close zero for wind speeds with low thrust coefficients.

2.1.2 Blade momentum theory

The profile of a wind turbine blade turbine can be compared with an airfoil when describing the forces that acts on the turbine, which is a representation of the cross section of the turbine blade. The two most fundamental forces are lift and drag force.

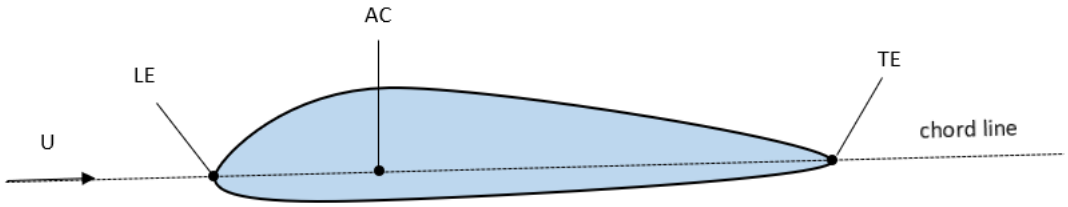

Figure 2.2: Airfoil of a wind turbine blade. This figure shows the leading edge LE, the aerodynamic center AC, the trailing edge TE, and the chord line, which is a straight line from the LE to the TE. This figure is inspired by Hansen [25].

When air moves towards the leading edge, the streamlines curve around the airfoil. The airfoil exerts a force on the air downwards. From Newton's third law, the air exerts an opposite force on the airfoil. This force in known as the lift force, and is perpendicular to the streamwise direction of the air flow. The lift force per unit span F_L is described as

$$F_L = \frac{1}{2}\rho c U_0^2 C_L \tag{2.9}$$

where c is the chord length and C_L is the lift coefficient. When a fluid is flowing over a body, it exerts a force on the body in the flow direction, termed as drag force. The drag force acts parallel to the streamwise direction of the air. The lift and drag force is illustrated in figure 2.3. The drag force F_D is described by the equation

$$F_D = \frac{1}{2}\rho c U_0^2 C_D \tag{2.10}$$

where C_D is the drag coefficient.

Figure 2.3 shows the different forces acting on and velocities around a wind turbine.

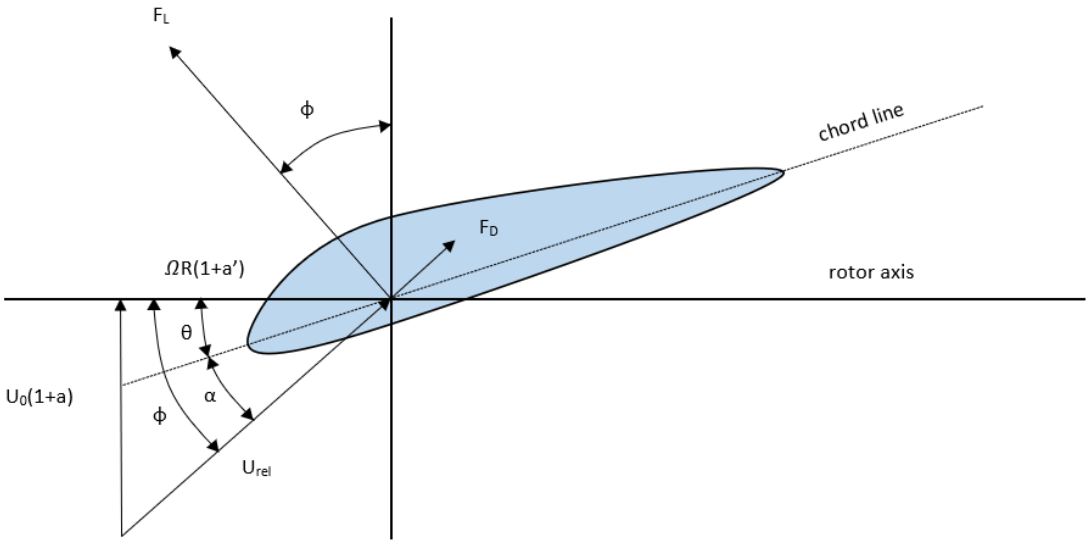

Figure 2.3: Profile of a a wind turbine with the most important forces and velocities action on a wind turbine blade. This figure is inspired by Manwell et al. [23].

The relative velocity U_{rel}, which is the inflow velocity, is parallel to the inflow angle ϕ. θ is the pitch angle, α is the angle of attach, α' is the angular induction factor, R is the rotor radius and Ω is the angular velocity. The pitch angle is important for regulation purposes of the wind turbine when the wind reaches rated wind speed.

2.1.3 Wind turbine regulation

The tip speed ratio, denoted TSR, is an important design parameter for wind turbines. It is given by the relationship

$$\lambda = \frac{\Omega R}{U_0} \tag{2.11}$$

where R is the radius of the rotor blade and Ω is the angular velocity of the rotor. It is important with a satisfying TSR, to achieve the highest possible C_p. The optimum tip speed ratio is often around 6-8 for a three-bladed HAWT [29].

The wind speed where the wind turbine starts to extract power is termed cut-in speed, usually around 3-4 m/s. The power extraction increases with cube of the wind speed, until it starts to flatten out. The wind speed where the maximum power output is reached is termed rated wind speed, with values typically from 11 - 17 m/s. The turbine extracts maximum amount of power between rated wind speed and cut-out speed, with a typical value of 25 m/s [30]. The wind turbine stops operating at wind speeds above this, to avoid extra loads, fatigue and damage on the turbine. The power curve as a function of wind speed for the turbine used in this study is presented in chapter 3.

2.2 The Atmospheric Boundary Layer

This section presents a general overview of how the atmospheric boundary layer is built up. Furthermore, a description of properties such as surface roughness and thermal effects are given, which are principal effects governing the properties of the atmospheric boundary layer. This section is intended as an introduction and a fundamental basis for the further reading about turbulence and the wake region behind wind turbines. This chapter is primarily based on the literature presented by Manwell et al. [23] and Burton et al. [24].

2.2.1 Nature of the wind

Wind is air in motion, which flows from a region with high pressure to a region with lower pressure. The pressure differences are caused by the differential surface heating of the earth, as a result of radiation from the sun. The different types of land and water surfaces absorbs the energy from the radiation differently. The air

rises in the atmosphere when it is heated and sinks when it is cooled. This leads to large-scale circulation patterns, influenced by the Coriolis force caused by the rotation of the earth. Obstacles like trees and houses have larger friction compared to the wind that blows over a smooth surface, which leach leads to reduced wind velocity.

2.2.2 Structure of the atmospheric boundary layer

The lowest level of the troposphere of the earth is known as the atmospheric boundary layer (ABL), or the planetary boundary layer. In this region of the troposphere, physical quantities such as temperature, air moisture and wind velocity are strongly influenced by the surface, and change rapidly in time and space. When investigating the wind resource at a specific site, the variation of the horizontal wind speed with respect to height is an important parameter. The wind speed is expected to increase exponentially with the height, and this variation of wind speed is called vertical wind shear.

The depth of the ABL strongly varies with temperature. It could range from a few hundred meters during the night due to surface nocturnal cooling, to 1-2 km during the day as a result of convective conditions. As an exception, the depth of the layer might reach 4-5 km over dry, hot surfaces [31].

The ABL is a turbulent layer, characterized by irregular swirls of motions, also called eddies. Turbulent eddy motions are primarily generated by two factors: forced convection and buoyancy. Forced convection occurs when air flow travels across rough objects such as grass, buildings and trees, and is forced to pass these. Buoyancy is a term used when warm air parcels are less dense compared to the surrounding colder air parcels, which creates a drift in the upward direction. Therefore, an important characteristic of the turbulence in the ABL is the effectiveness related to transportation of heat, moisture and natural greenshouse gases. A comprehensive description about turbulence will be carried out in chapter 2.3 for deeper understanding.

2.2.3 Atmospheric stability

The thermal state of the ABL can be divided into three categories, which are stable, unstable and neutral. The ABL is unstable when the surface is heated, making warm air near the surface to rise. When the air rises, the pressure is

reduced, the air expands, and cools adiabaticaly. If the effect of the cooling is too small to bring the rising air into thermal equilibrium with the surrounding air, the air will keep rising, which leads to large convection cells. The result of this is a thick boundary layer with large-scale turbulent eddies, typically with a depth of 1-2 km as mentioned earlier.

The ABL is stable when the vertical motion of the rising air is suppressed due to adiabatic cooling, which makes the raising air to become colder than the surroundings. This is often the case during cold nights, when the surface is cooled. This situation is characterized with large wind shear, and the turbulence is generated by the surface friction.

For the situation with the neutral ABL, the raising air remains in thermal equilibrium with the surroundings because of the effect from adiabatic cooling. This is typical in strong winds, where the turbulence is generated by the surface roughness. Neutral stability is important for wind energy applications, since strong winds generate most energy because the turbines will operate within the rated power regimes. This will also cause the highest loads on the turbines.

The most common parameter to characterise atmospheric stability is known as Monin-Obukhov length described by:

$$L = -\frac{T_0 u_*^3}{\kappa g \sqrt{\overline{\omega' \, T'}}} \tag{2.12}$$

where T_0 is the mean temperature of the layer, g is the gravitational acceleration constant, $\overline{\omega' \, T'_0}$ is the kinematic virtual heat flux of the surface layer and u_* is the friction velocity.

The Monin-Obukhov length is a length scale, which describes the height of the sub-layer of dynamic turbulence. A further description is found in Obukhov [32], Monin and Obukhov [33], Sempreviva et al. [34] and Foken [35]. The sign of the Monin-Obukhov length indicates the classification of the atmospheric stability, where a minus sign indicates unstable atmosphere, near zero indicates stable, and positive indicates neutral. Classifications such as very unstable, near unstable, near-neutral, near stable and very stable are also found in the literature, see Pena et al. [36]. Barthelmie et al. [37], Barthelmie and Jensen [38], Wharton and Lundquist [39] and Keck [19].

In one of these studies [38], Barthelmie and Jensen found that near-neutral conditions dominates the ABL for wind speeds exceeding 15 m/s. Furthermore, they

showed that for wind speeds ranging from 5-10 m/s, roughly 20% of the cases are classified as neutral class, 40% as stable, and 40 % as unstable.

The wake is affected by the level of atmospheric stability, and a number of studies have presented how this affects the power production, see Hansen et al. [25], Barthelmie et al. [40], Alblas et al. [41] and Keck [19]. How the wind turbine loads are affected by the atmospheric stability is investigated by Sathe and Bierbooms [42], Sathe et al. [43] and Kotur and Đurišić [44].

2.2.4 Velocity profiles

As mentioned earlier, the wind velocity increases with height due to the friction of the surface. This change happens more rapidly close to the surface. This can be expressed in many ways, but the most common is known as the power law, expressed as:

$$U(z) = U_{ref}\left(\frac{z}{z_{ref}}\right)^{\alpha} \tag{2.13}$$

where $U(z)$ is the wind velocity is in a given height z, U_{ref} wind velocity in a given reference height z_{ref}, and α is the power exponent. According to Emeis and Turk [45], the power law is often used for wind energy purposes due to its mathematical simplicity. There is also a different, simple approach for the modelling of wind speed as a function of height, described by:

$$U(z) = U_{ref}\left(\frac{ln(z/z_0)}{ln(z/z_{ref})}\right) \tag{2.14}$$

where z_0 is the surface roughness length. The surface roughness offshore is typically around 0.0002m, about hundred times less than the smallest roughness length onshore [46]. However, since the usefulness of these two equations are limited, a more complex equation is used for the modelling of the wind speed with respect to height. This is known as the logarithmic wind profile function, and is used in this study. It is described by the relation

$$U(z) = u_*\left(\frac{ln(z/z_0) + \Psi}{\kappa}\right) \tag{2.15}$$

where $\kappa = 0.4$ is the von Karman constant, and Ψ is a function that depends on the stability. It is positive for stable conditions, which gives high wind shear, and negative for unstable conditions, which gives low wind shear. In neutral conditions, Ψ is often neglected since this term becomes very small compared to the first term. Nevertheless, Ψ is solved numerically based on the method described by Stull [47] in this thesis. The roughness length is calculated by the following formula:

$$z_0 = z_{ch}\frac{u_*^2}{g} \tag{2.16}$$

where z_{ch} is known as the Charnock constant, where a value of 0.018 is used, based on the findings by Wu [48].

2.3 Turbulence

This chapter gives a review of the distinct features of turbulence. A brief introduction of the nature of turbulence will be presented, before a more detailed description about the different statistical properties of turbulence is presented, such as turbulence intensity, the normal distribution, turbulence length scale and turbulence spectra. This section is primarily based on the literature described by Burton et al. [24] and Manwell et al. [23].

2.3.1 Nature of turbulence

Turbulence can be described as irregular movements of a fluid, characterized by random and and chaotic three-dimensional vorticity [49]. Turbulence in the ABL is primarily generated by thermal effects and surface friction. Examples of turbulence generated by friction is when the wind hits a building or a three, creating an irregular motion of the wind behind the obstacles. Friction and generated turbulence are often connected, for example when the air flows over a mountain ridge, the air is no longer in thermal equilibrium with the surroundings [24].

Turbulence is dependent of time and space. The three-dimensional movement of the air can be decomposed to a longitudinal, lateral and vertical component. The longitudinal component is defined to be in the prevailing wind direction, $u(z,t)$. The lateral component is denoted $v(z,t)$, and the vertical component $w(z,t)$, where

z is the height and t is the time. Each component can further be divided into two parts, the fluctuating part of zero mean, u_{mean}, and the average short - term wind speed, U_mean. The expression for the instantaneous wind speed in the longitudinal direction is thus described by:

$$u = u_{mean} + U_{mean} \tag{2.17}$$

The same relation is valid for the wind in the lateral and vertical direction. The dependence of z and t is not shown due to simplicity reasons. The short-term average longitudinal wind speed, U_{mean}, is often averaged over a time period of ten minutes, and usually not more than an hour. Instantaneous turbulent wind is not observed continuously in practice, but is sampled with a sufficiently high rate. The turbulent wind can then be described by the equation:

$$U_{mean} = \frac{1}{N}\sum_{i=1}^{N} U_i \tag{2.18}$$

where U_i is a sequence of longitudinal the wind speed, and N is the number of sequences during the time period.

Since turbulence is a property of temperature, pressure, density, and the movement of air in a three dimensional space, it may be expressed by a set of differential equations. However, small differences in the initial conditions may lead to severe differences in the calculations over a relatively short time period. Hence, statistical methods is a common way to describe turbulence. The next subsections in this section present some of the most important statistical characteristics for wind energy modelling.

2.3.2 Turbulence intensity

Turbulence intensity, TI, is the most important statistical property when describing the behaviour of turbulence in the ABL, and is described by the relation:

$$TI = \frac{\sigma_u}{U_{mean}} \tag{2.19}$$

where σ_u is the standard deviation of the longitudinal wind speed U about the

mean wind speed U_{mean}. There is a corresponding notation for the turbulence intensity for the lateral and vertical direction. As mentioned earlier, the wind speed increases when the roughness is reduced. Hence, the turbulence intensity is usually reduced with respect to height, since the wind speed increases with height in the ABL, and the standard deviation stays nearly constant [23].

There are several studies which have documented the effect of the distribution of turbulence intentity in the ABL with respect to wind speed, see Carpman [50], Barthelmie et al. [40] and Hansen [25]. Their measurments shows that the turbulence intensity is highest for the first turbine in the row, decreasing deeper inside the wind farm. Furthermore, it was found by Hansen et al. [25] that smaller turbulence intensity gives increased wake losses. Furthermore, Barthelmie and Jensen found that the turbulence intensity for wind speeds above 5 m/s in a height of 69 m in Nysted wind farm is 0.046 in stable conditions, 0.060 in neutral conditions, and 0.064 in unstable conditions, with an average turbulence turbulence intensity of 0.056 [38]. It was also found by Barthelmie [37] that high wind speeds are often are associated with a near-neutral stability class. Furthermore, Keck [19] and [51] showed fine agreement with simulations of the DWM model compared to field measurements in Lillgrund wind farm, with a simulated turbulence intensity of 6.2% in neutral conditions.

2.3.3 Probility density function

Turbulent wind may seem chaotic, but follows a pattern. A classical assumption is to describe the turbulent wind speed about the mean wind speed U_{mean} with the probability function of the normal distribution, also known as the gaussian distribution. This is given by the equation:

$$p(u) = \frac{1}{\sigma_u \sqrt{2\pi}} e^{\frac{-(u-U_{mean})^2}{2\sigma_u^2}} \tag{2.20}$$

where $p(u)$ is the probability that a given wind speed u will occur, based on a given U_{mean} and σ_u. It is given from the Gaussian distribution that 68 % of the occurrences are within one within standard deviation $_u$ to both sides of U_{mean}.

2.3.4 Integral time scale and integral length scale

Integral time scale provides a measure of the average time over which wind speeds are correlated. A measure of the extent of the region over the correlated velocities is known as the integral length scale. This means that the integral time scale provides a measure of the average size of the eddies. The integral length scale is usually more constant over a wider range of wind speeds compared to integral time scale, which makes it more representative for a site. Two other important statistical methods for estimation of turbulence is the power spectral density function, and autocorrelation, which are not discussed in this study.

2.3.5 Turbulence spectra

A spectrum of turbulence describes the frequency content of wind-speed variation. Two common turbulence spectra is the Kaimal spectrum, and the von Karman spectrum. For this thesis, the von Karman spectrum is used to model the frequency content of the wind speeds, which is important for the implementation of the meandering of the wake, where the Mann turbulence model is used, described in [52] and [53]. This is further explained in section 2.5.

The von Karman spectrum is given by the following relation, originally described by von Karman [54]. A similar notation as used in the equation below is presented by Mann [52]:

$$E(k) = \alpha\epsilon^{\frac{2}{3}} L_u^{\frac{5}{3}} \frac{(L_u k)^4}{(1 + (L_u k)^2)^{\frac{17}{6}}} \tag{2.21}$$

where $E(k)$ is the energy spectrum, $\alpha \approx 1.7$ is known as the Kolmogorov constant, k is the wave number, ϵ is the rate of viscous dissipation of specific turbulent kinetic energy and L_u is a length scale in the longitudinal direction.

2.4 Wind turbine wakes

This section presents a description of the wake behind wind turbines, particularly the development of the wake deficit, and a categorization of the different wake regions. Furthermore, a description of the wake meandering process is given,

which provides a foundation for the description of the DWM model presented in section 2.5

2.4.1 Wake deficit

The wake is the region behind the wind turbine, where the wind velocity has decreased compared to the free-stream velocity, because kinetic energy has been extracted from the wind by the wind turbine. The wake is characterized by increased turbulence compared to the free-stream wind, and turbines operating in the wake of another turbine produce less power, and experience greater loads as a result of these factors. Hence, the loss of momentum and the velocity reduction of the wind is directly related to the trust coefficient, defined in equation 2.8. It was found by Moskalenko et al. [55] that the annual energy reduction in a wind farm was 12 % due to wake losses, which is in fine agreement with a estimate of $10 - 20\%$ for large offshore wind farms according to Barthelmie et al. [56].

The wake is usually divided into three regions, the near wake, intermediate wake and far wake. Each region requires different modelling approaches, as the atmospheric conditions varies greatly between the regions.

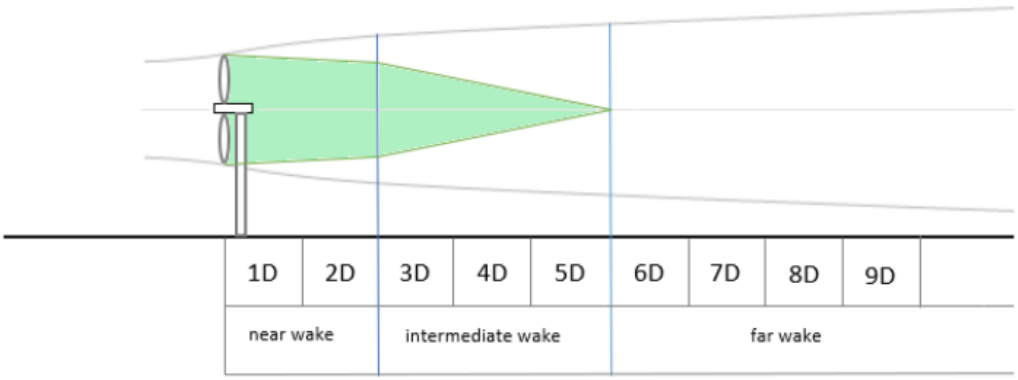

Figure 2.4: Illustration of near, intermediate and far wake region, where the distance with respect to the rotor diameter is shown along the x-axis. This figure is inspired by Eecen et al. [57].

From figure 2.4 it is seen that the wake width is slightly larger than the turbine diameter and slowly increasing with distance downstream. This is a result of the

wind speed gradient from the wake and the free wind speed outside the wake, leading to a shear generated turbulence. The white region between the grey lines defining the wake region, and the green region shown in figure 2.4 is known as the wake shear layer. There is a large pressure drop in the wind over the rotor, which gradually approaches the ambient pressure downstream [27]. The location where the pressure in the wake has reached the ambient pressure level is defined as the end of the near wake in this thesis, and has the length of 1-2 rotor diameters [57].

As illustrated in figure 2.4, the wake shear layer expands inwards to the wake center as well as outwards. After 2-5 rotor diameters, wake shear layer has reached the wake center, and the turbulence and velocity distribution approaches Gaussian shape according to Crespo et al. [58]. This is defined to be the end of the intermediate wake region is in this thesis.

As seen in figure 2.4, the wake width expands approximately linearly with downstream distance in the far wake region, slowly becoming wider but shallower until the flow fully recovers downstream. The velocity and turbulence profiles are approximately of Gaussian shape. The wake from entire wind farms often extends to 10-15 km, but it has been observed to be up to 55 km with satelite measurements according to Hasager [59]. This indicates that wakes is not only an important issue regarding the interaction between turbines in a wind park, but also between wind farms with close spacing, investigated by Nygaard [60].

2.4.2 Wake meandering

The term wake meandering refers to large-scale movement of the entire wake, characterized by oscillations in all directions. The meandering phenomenon of the wake is not yet fully understood and is currently an ongoing research topic. This is an interesting topic due to the fact the meandering effect gives gives increasing structural loads, resulting in reduced life-time of the turbines. This is described further in section 2.5, and in detail by Larsen et al. [16] and Madsen et al. [17]. It was found experimentally by España et al. [61] that the magnitude of the wake meandering increases with increasing turbulence intensity. This has been confirmed numerically by Keck et al. [62].

2.4.3 Wind farm effect and wake merging

The placement of wind turbines in a wind farm and the incoming wind direction are important factors for the development of wake formation and wake recovery. The term wake merging is used when several wakes interact. This is also termed as a multiple wake situation. There is a distinction between lateral wake merging, and downstream wake merging, illustrated by figure 2.5.

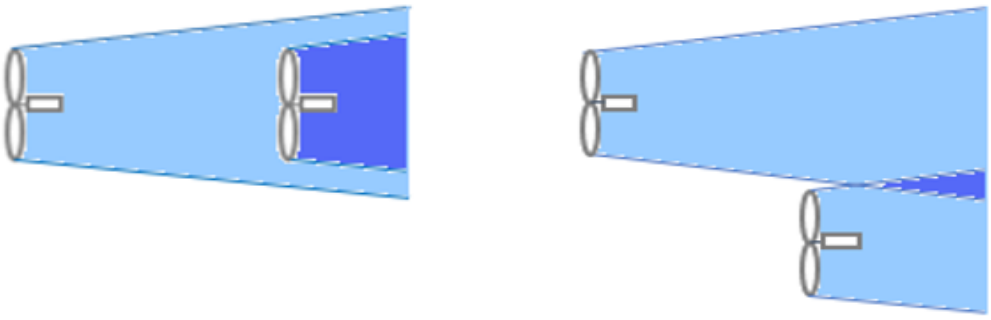

Figure 2.5: Downstream wake merging and lateral wake merging. This figure is inspired by Trabucchi et al. [63].

Downstream wake merging occurs when the wake from an upstream turbine reaches a downstream turbine, which results in a combined wake, released from the downstream turbine. Lateral wake merging occurs when there is an interaction between wakes from parallel turbines, as seen in figure 2.5. This might occur deep inside wind farms as seen in figure 2.6, which is a very famous photo in the wind industry.

Figure 2.6: Wakes in Horns Rev wind farm [64].

Downstream wake merging and lateral wake merging is clearly observed. Rare atmospheric conditions with very humid air made it possible to visualize the wake and turbulence patterns behind the wind turbines [64].

Downstream wake merging is further separated into full wake merging and partial wake merging. The term full wake merging is used when the ambient wind is perfectly aligned with the turbine row, and partial wake merging is used when there is an offset between the angle of the ambient wind speed and the row of wind turbines. In this thesis, only aligned cases and thus full wake merging are investigated. According to Barthelmie et al. [26], the wake losses are maximized in full wake merging cases below rated wind speed, where the thrust coefficient is high.

For large wind farms, the wake may have merged laterally for rows deep into the farm as observed in figure 2.6. As a result of the lateral wake merging, there is a reduction in the horizontal wake recovery, and most of the momentum from the ambient air flow enters the wake vertically. For this reason, the power production for a turbine placed deep inside a wind farm tends to decrease, compared to the nearest upstream turbine. This is known as the deep array effect, and is invest-

igated by Barthelmie et. al [38], Frandsen [65], Nygaard [60], and Brower et. al [66].

2.5 Dynamic Wake Meandering Model

As mentioned previously, the dynamic wake meandering model, referred to as the DWM model, may be used to simulate the structural loads and the power production from each of the individual turbines in a row inside a wind farm. The DWM model is divided into three fundamental parts, as shown in figure 2.7:

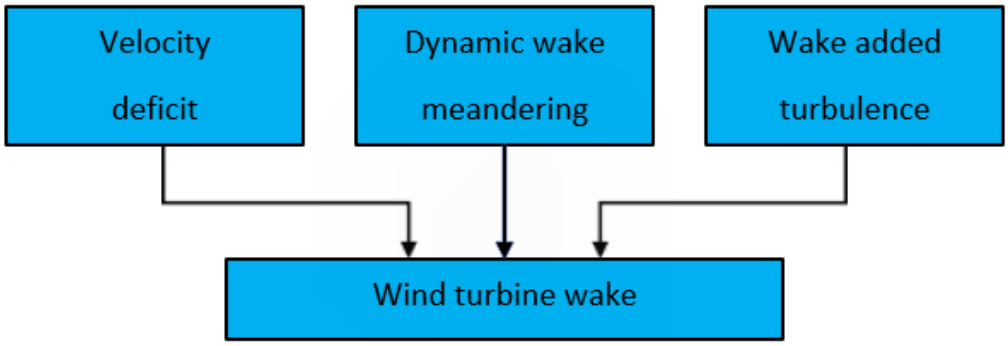

Figure 2.7: Schematic figure of the DWM model, inspired by Madsen et al. [17]

1: Modelling of the quasi-steady velocity deficit

2: A stochastic model of the wake meandering process

3: A model of the added or self-generated turbulence.

A fundamental assumption in the DWM model is that these three parts are modeled independently. Below, a brief description of the DWM model is presented. A further description of the fundamental assumptions and a more detailed description of each of the three parts of the model is presented by Larsen et al. [16] and Madsen et al. [17].

2.5.1 Velocity deficit

The quasi-steady velocity deficit is formulated in the meandering frame of (MFoR), and expansion of the wake is included as a function of the transportation time downstream, caused by turbulence diffusion. MFoR refers to a coordinate system relative to the global.

The modeling is based on a thin-shear layer approximation of the Reynolds averaged Navier-Stokes equations in rotational symmetric form, combined with an eddy viscosity model, based on the work from Ainslie [14]. The balance for momentum and continuity is maintained by:

$$\frac{1}{r}\frac{\partial}{\partial r}(rV(r,x)) + \frac{\partial U_a\,(r,x)}{\partial x} = 0 \tag{2.22}$$

$$U_a\frac{\partial U_a(r,x)}{\partial x} + V(r,x)\frac{\partial U_a(r,x)}{\partial r} = \frac{\mu_T}{r}\frac{\partial}{\partial r}(r\frac{\partial U_a(r,x)}{\partial r}) \tag{2.23}$$

where U_a is the velocity in the axial direction x, V is the velocity in the radial direction r, and μ_T is the eddy viscosity. This is a simplification due to the neglected pressure term and the reduction of the momentum equation in accordance to the full set of Navier-Stokes equations. The eddy viscosity consists of both the contribution from the ambient turbulence, which is represented by the left side of equation 2.28, and the contribution from the mixing length description due to the shear layer of the wake deficit is represented by the right side of equation 2.28. The non-dimensional eddy viscosity is described as:

$$\mu_T^* = k_1 F_1 I_a + k_2 F_2 R_w \left(1 - \frac{U_{\min}}{U_0}\right) \tag{2.24}$$

F_1 and F_2 are filter functions included to govern the development of the turbulence stresses, with the purpose of limiting the turbulence in the wake before there equilibrium is achieved between the wind field and turbulence field. This eddy viscosity formulation is described by Madsen et al. [17]. However, F_1 has later been re-calibrated, described by Larsen et al. [18], and that version of F_1 is implemented in this study. k_1 and k_2 are empirical constants, $k_1 = 0.07$ and $k_2 = 0.008$, which are used to calibrate the wake deficit. U_0 and I_a are the ambient wind speed and ambient turbulence intensity at hub height. R_w is the radius of the wake, and U_{min} is the minimum wind speed in the wake cross-section.

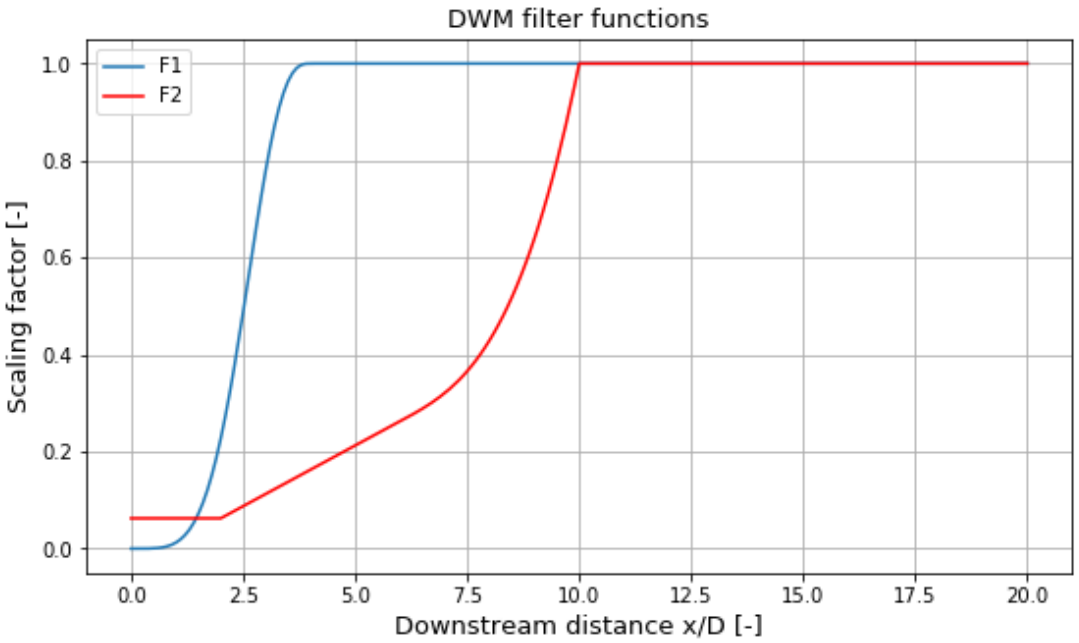

Figure 2.8: Filter functions applied to the eddy viscosity formulation

Figure 2.8 shows the development of the filter functions as a function of downstream distance. As seen for F_2, it starts increasing after a distance of 2D, which is the end of the near wake, where the pressure has recovered to ambient level. These filter functions are presented in IEC standard [21].

2.5.2 Wake meandering

The wake meandering part is based on a fundamental presumption, stating that the wake in the ABL can be modelled as passive tracers, driven by large-scale atmospheric turbulence, in lateral and vertical direction. This effect is accounted for in the order to perform simulations of the flow field in the fixed frame of reference (FFoR), which refers to a coordinate system relative to the wake center. An appropriate description of the stochastic transport velocity of the wake and a definition of a suitable cut - off frequency defining the large-scale turbulence structures is needed to model the wake meandering process.

For the stochastic modelling of wake meandering, the wake is imagined to be constituted by a cascade of wake deficit elements. Each of these elements are released from the turbine at consecutive time instants, in agreement with the passive tracer

analogy [16]. Taylor's hypothesis states that the downstream advection of the wake deficit elements controlled by the mean wind speed of the wake. Adopting this hypothesis, the wake momentum becomes invariant with respect to the longitudinal wake displacement, in direction of the mean wind flow. This is a significant simplification, allowing a decoupling of the wake and the wake transportation [16]. The displacement of the considered wake deficit element in lateral and vertical directions are calculated based on large-scale turbulent velocities, at each time instant. The dynamics of the wake cascade elements are thus described mathematically by the following first order differential system:

$$\frac{dy\left(t,t_0\right)}{dt} = v_c\left(y,z,t,t_0\right), \tag{2.25}$$

$$\frac{dz\left(t,t_0\right)}{dt} = w_c\left(y,z,t,t_0\right) \tag{2.26}$$

where v_c and w_c are the spatially dependent large-scale turbulent velocities in the lateral direction y and the vertical direction z respectively, and t_0 is the time instant at which each considered wake cascade element is emitted [67].

The large-scale turbulent structures are limited to a minimum characteristic length scale of two rotor diameters, as the turbulent eddies smaller than $2D_w$, where D_w denotes the diameter of the wake, tends to contribute more to the velocity deficit rather than the meandering process. Hence, a low pass cut-off frequency filter is therefore introduced to extract the large large-scale turbulent eddies that contributes to the meandering process, which excludes eddies smaller than $2D_w$ [16]. This cut-off frequency is defined as

$$f = \frac{U_0}{2D_w} \tag{2.27}$$

Based on the description above, the meandering is implemented in the code by the following numerical scheme:

1. Generate a turbulence box. The synthetic turbulence is modelled according to Mann turbulence model, described by Mann [52], [53]. In this study, the turbulence box has a length of $N_x = 4096$ grid points in the axial direction, where length of the box in the lateral and vertical direction is $N_y = 32$ and $N_z = 32$ grid points.

2. Calculate the average of all fluctuations over the cross-section of the wake, which increases along the axial direction.

3. The wake segments are released with a time separation $dt = 1.0s$. The meandered wake moves downstream with a wake velocity of 80% of the ambient velocity, which gives the expression $u_w = 0.80U_0$.

4. Calculate the velocities in axial, lateral, and vertical direction.

5. The positions of the wake segments are updated as following:

$$dx = (u_w)dt \tag{2.28}$$

$$dy = v_w dt \tag{2.29}$$

$$dz = w_w dt \tag{2.30}$$

2.5.3 Wake added turbulence

The purpose with the wake added turbulence formulation of the DWM model is to account for the increased level of small-scale turbulence vortices in the wake region. A well as the formulation of the wake deficit, the wake added turbulence is supposed to be in the meandering frame of reference. An important contribution to wake added turbulence is mechanically generated turbulence, which is caused by the wake shear, in addition to the tip and root trailing vortices. These vortices will gradually break down and approach the characteristics similar to conventional turbulence. A more detailed description is found in Madsen et al. [17]. The increased turbulence results in increased fatigue loads for the downstream turbines. It was found by Keck [19] that by including wake added turbulence and turbulence build-up over a row of turbines, the wake losses were reduced by 9% for a row with 6D turbine spacing. This illustrates the importance of a comprehensive turbulence formulation.

2.5.4 Wake modelling

Originally, the DWM model is based BEM theory, where blade data consisting of tables including twist angles and chord length as a function local radius are used to model the forces on the blade, and the velocity in the near wake. The equations modelling the evolution of the wake is described by Madsen et al. [17]. Unfortunately, such blade data could not be provided for this study. As a result of this, publicly available C_P and C_T tables as functions of wind speed together with the assumption of Gaussian velocity profiles were used instead.

The length of the near wake is modelled by an empirical approach divided into two regions, based on Lange et. al [68]. The first region x_H is given by the relation:

$$x_H = r_0 \left[\left(\frac{dr}{dx}\right)_a^2 + \left(\frac{dr}{dx}\right)_\lambda^2 + \left(\frac{dr}{dx}\right)_m^2 \right]^{-\frac{1}{2}} \tag{2.31}$$

The first term in the square bracket represents the contribution from the ambient turbulence, the second term rotor generated turbulence, and the third term shear-generated turbulence. r_0 is the fully expanded radius of the rotor disc. Finally, the total length of the near wake x_n is calculated with the following expression:

$$x_n = \left(\frac{\sqrt{0.212 + 0.145m}}{1 - \sqrt{0.212 + 0.145m}} \right) \left(\frac{1 - \sqrt{0.134 + 0.124m}}{0.134 + 0.124m} \right) x_H \tag{2.32}$$

where m is given by the relation:

$$m = \frac{1}{\sqrt{1 - C_T}} \tag{2.33}$$

The expansion of the wake radius and the wake velocity profile is calculated with equations based on the work of Ainslie [14], and is also presented by Waldl [69], and partly by Lange [68]. A Gaussian velocity profile for the wake expansion R_w is assumed, formulated as:

$$R_w = \sqrt{\frac{3.56 C_T}{4 U_d \left(2 - U_d\right)}} \tag{2.34}$$

U_{d0} is the centerline velocity deficit 2D behind the rotor, normalized with the free-stream velocity. This is dependant of the thrust coefficient and ambient turbulence, and is based on a study of rotors in wind tunnels, given as:

$$U_{d0} = C_T - 0.05 - (16C_T - 0.5)\,\frac{I_a}{10} \tag{2.35}$$

The centerline velocity deficit profile U_d, is modelled according to Ainslie [14] by:

$$U_d = U_{d0} e^{-3.56\left(\frac{r}{R_{w0}}\right)^2} \tag{2.36}$$

where R_{w0} is the initial wake radius.

Chapter 3

Method

3.1 Lillgrund offshore wind farm

Lillgrund wind farm is the biggest swedish offshore wind farm, located in the Øresund strait between Denmark and the southwest coast of Sweden. The wind farm consists of 48 SWT-2.3-93 pitch-controlled turbines manufactured by Siemens. With rated power of 2.3 MW for each turbine, the total rated capacity of the farm is 110 MW. According to Peder Enevoldsen from Siemens Gamesa, recent evaluations has been conducted on the Lillgrund turbine, concluding that the hub height of the SWT-2.3-93 turbines is 68.8m. The rotor diameter is 93m. Further information is found in [70] and information about Lillgrund is also presented by Gögmen and Giebel [71].

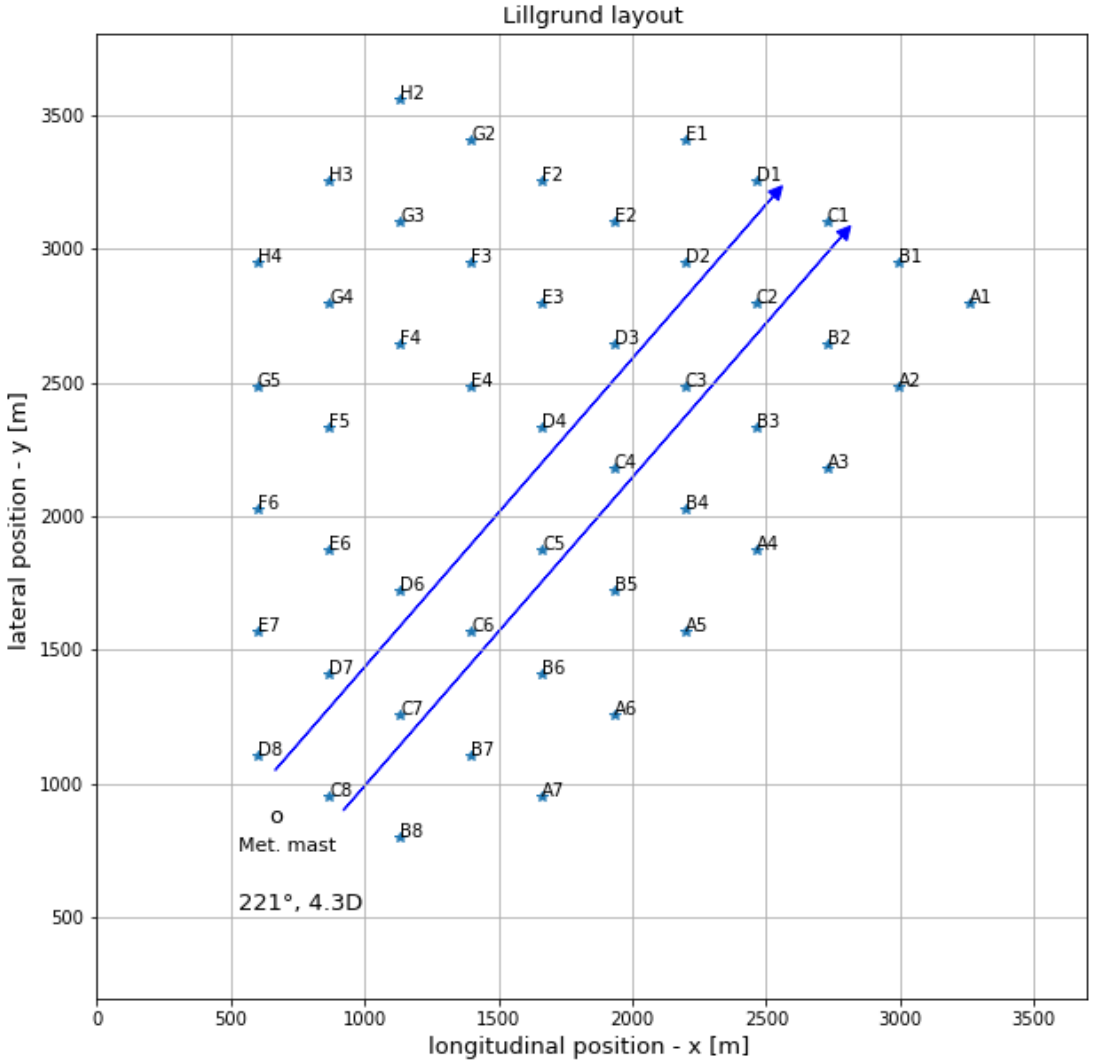

Figure 3.1: Layout of Lillgrund wind farm, with the investigated cases highlighted.

As seen in figure 3.1, the layout of the farm is quite unusual, with a small turbine spacing and a gap in the middle of row D and E, where two turbines should have been placed. The reason behind this is the fact that the water is too shallow to access for construction boats here. As a result of this, the turbine spacing between turbine D6 and D4, and E4 and E6, is 8.6D. This affects the wake recovery and power production of the turbines downstream of this gab. Figure 3.1 shows that the spacing between the turbines in row A-H is 4.3D. The spacing between the turbines in row 1-8 is 3.3D.

The power and thrust curve of the SWT-2.3-93 turbines of the site are shown in figure 3.2. This power coefficient curve, thrust coefficient curve and power curve is based data found in [70].

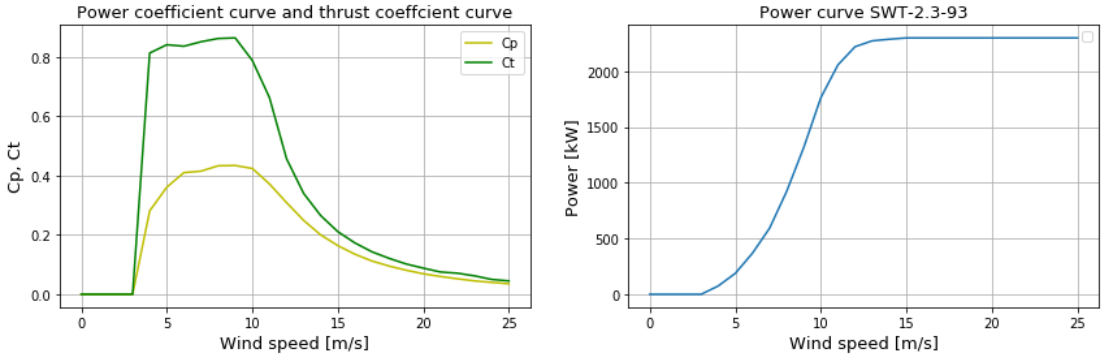

Figure 3.2: Power coeffcient curve, thrust coefficent curve and power curve of the SWT-2.3-93 turbine.

Figure 3.2 shows that cut-in wind speed for the turbine is 3.5 m/s, the rated wind speed is 13 m/s, and the cut-out wind speed is 25 m/s. Moreover, the figure shows that the thrust coefficient is kept above 0.80 from 4-9 m/s, and decreases rapidly from 10 m/s with increasing wind speeds.

3.2 Velocity deficit

Before the modelling of the wake merging takes place, velocity and power for the second turbine in the row is calculated. The deficit from first turbine is found by calculating the velocity field in the wake of the first turbine at a distance corresponding to the distance between the first and the second turbine, assuming free-stream velocity in accordance with the modelling procedure described in section 2.5. Further, the velocity deficit is found by taking the free-stream velocity minus the averaged wake velocity over the swept area of the second turbine.

3.3 Calculation of multiple wakes

There are several different methods for modelling wake merging, where a description of the most common methods are presented by Machefaux et al. [72]. Two of these methods are now implemented in the current IEC standard [21], where one gives the best results for the wind regime below rated, and the second for the wind regime above rated. In this study, three different methods are compared.

3.3.1 Dominant wake approach

This wake merging method is currently the standard approach for the wind regime where the power production is below rated power, described in [21], [73], and [18]. This approach assumes that the incoming flow of a turbine operating in the wake of multiple upstream turbines is found by picking the dominating deficit from all the wakes at each point over the rotor area. It is defined as:

$$U_w\left(r,\theta,t|x\right) = MAX_i\left(U_{w,i}(r,\theta,t|x\right) \tag{3.1}$$

$U_{w,i}$ denotes the wakes from all the upstream turbines, x is the longitudinal position located of the investigated downstream turbine, t denotes a temporal coordinate and (r,θ) is the polar coordinates in the rotor plane. Figure 3.3 below illustrates the wake merging method for this approach.

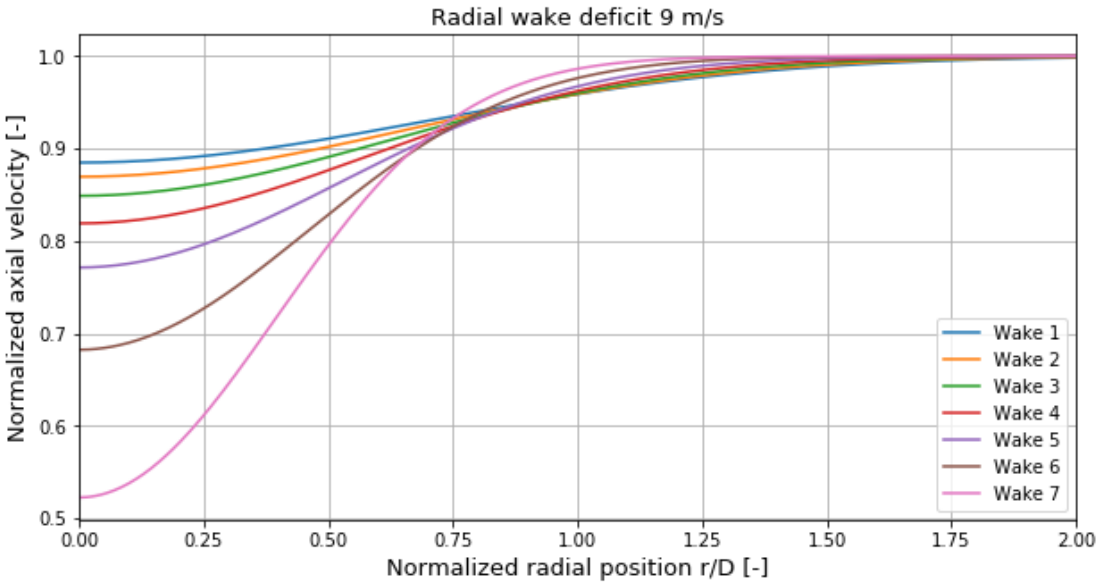

Figure 3.3: Radial wake deficit at 9 m/s, seen at the position of 4.3 diameters behind the seventh turbine, in a row with seven turbines and a turbine spacing of 4.3D.

The MAX method is modelled by calculating the wake from $-0.5 \leq r/D \leq 0.5$. Based on this, an imaginary last turbine in the row would be affected by the wake from turbine number 7, since the wake from this turbine is the dominating wake deficit at all points in the rotor area.

3.3.2 Linear summation

This wake method is based on a simple linear superposition of the wakes. This method is further denoted SUM in this thesis. It is the implemented in IEC-standard for the wind regime above rated wind speed, and described in [72], [21], [73] and [74]. With the same notation as described for the dominant wake approach, the linear summation approach is modelled by the expression:

$$U_w\left(r,\theta,t|x\right) = \sum_i \left(U_{w,i}(r,\theta,t|x)\right) \tag{3.2}$$

3.3.3 Quadratic summation approach

The quadratic superposition, denoted SQR in this thesis, is widely used in the Park program [75], and also used by Nygaard [60]. These are based on the Jensen model, although the summation method is also applicable for other wind engineering models, like the DWM model. It is obtained by taking the square root of the sums of the upstream single wakes. The quadratic summation approach is given by the relation:

$$U_w\left(r,\theta,t|x\right) = \sqrt{\sum_i \left(U_{w,i}(r,\theta,t|x)\right)} \tag{3.3}$$

3.4 Simulated cases and field data

Table 3.1: Overview of the simulated cases and the input parameters used in the simulation. The bin size only applies for the field data.

Case	Number of turbines	Turbine spacing	TI	Bin size	Vel. range
Row C	7	4.3D	6.0	±6°	9-17 m/s
Row D	7	4.3D	6.0	±6°	9-17 m/s

Table 3.1 shows the most essential information about the simulations, where the number of turbines, turbine spacing, TI and the the free-stream velocity, denoted Vel. range in the table, illustrating the range of velocities simulated, is used as input for the DWM model. The bin size only applies for the field data. It is important to note that the bin size in the table only applies for the downstream turbines, and not the upstream turbine in each row. The accepted bin size for the upstream turbine in each case, C8 and D8, is ±2.0°. Since the DWM model is simulated as a perfectly aligned case, it is desirable with a as small inflow bin angle as possible for the field data. Nevertheless, it was not possible to keep this bin size for the downstream turbines, since it would not be possible to gather enough measurements from the field data with a bin size this small. Furthermore, all the simulations are conducted with a neutral stability class. Additionally, there could not be obtained enough measurements for certain wind speeds around rated wind speed for turbine C8, within the required bin angle. Turbine C8 was therefore excluded from the simulations. Running the simulations with a turbulence intensity

of 6.0% at neutral stability class is supported by measurements from Barthelmie et al. [38]. Furthermore, Madsen et. al [76] showed fine results with a TI of 6.0% used in the simulations for the power prediction at various wind speeds in Lillgrund.

The data used for the simulations cover a period of 8 month, ranging from 03/2012 to 10/2012, and each measurement is 10 min averaged. The measured power for each turbine is filtered based on the wind direction bin angle presented in the previous subsection, and for the wind speeds investigated for each case. The power production is investigated by nine wind speeds for each row, ranging from 9 - 17 m/s. For all the cases, wind speeds within an interval of ± 0.5 m/s is included for each case, for example 13 ± 0.5m/s. The filtered measurements were gathered, and the average wind speed and power of the extracted measurements is calculated. Moreover, measured power from the individual turbines were excluded if the turbine did not produce any power. Nine of the turbines positioned in the southern part of the wind farm, are curtailed for some of the measurements. This includes three of the turbines positioned in row C and D. The measurements with curtailment are thus excluded.

Chapter 4

Results

.

4.1 Power production

This chapter presents the results from the simulations of row C and D in Lillgrund with three different wake summation methods, compared with field data. The red-dashed line is field data, the blue line visualizes the MAX method, the green line visualizes the SQR method, and the orange line visualizes the SUM method at the various wind speeds.

4.1.1 Row C

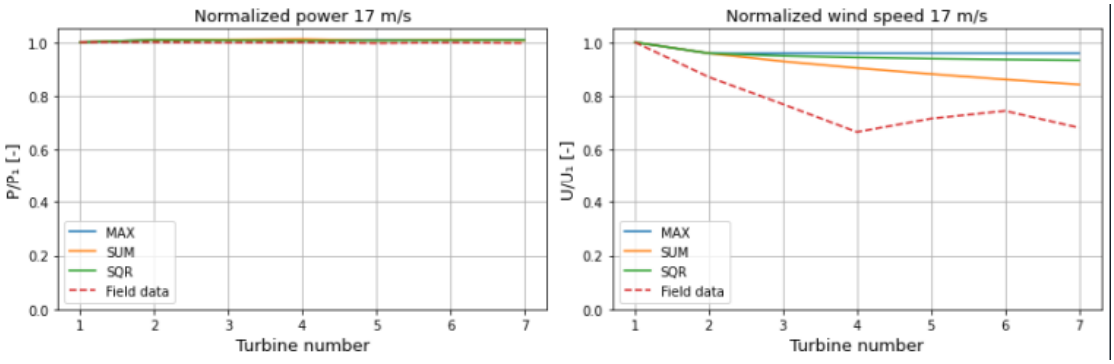

Figure 4.1: Normalized power and normalized wind speed at 17 m/s

As seen in figure 4.1 for the normalized wind speed, the wind speed decreases almost linearly until turbine 4, where there is a small increase in wind speed. Despite the fact that the wind speed is reduced with about one third at turbine four, the power production is still at rated power, as seen in figure 4.1. Hence, the normalized power production does not provide any information about the wake losses. As there is a larger wake wake loss in rear part of the row, compared to turbine 2, the SUM methods captures this effect best, with reduction of approximately 0.10 from turbine 2. However, there is a large difference between the simulations and the field data, which already occur at turbine 2. This corrupts the result to some degree. This is not a result of the different wake merging methods, but the modelling of the velocity deficit. This will be discussed in chapter 5.

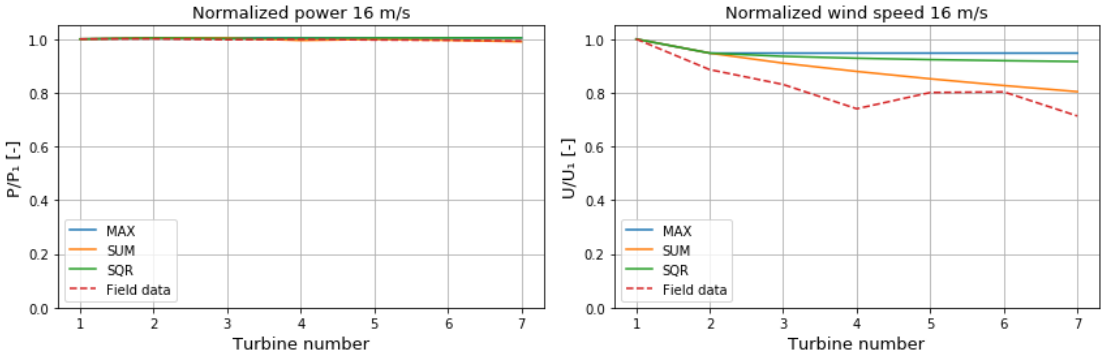

Figure 4.2: Normalized power and normalized wind speed at 16 m/s

The situation at 16 m/s second shows a similar pattern as the one for 17 m/s,

although the measured velocity deficit is lower for all of the turbines, and the estimated velocity deficit is slightly larger. For this situation, there is a reasonably fine agreement between the SUM method and the field data, where the SUM method captures the small linear decrease of the wind speed. However, figure 4.2 shows that the SUM method overestimates the wind speeds with an average of about 0.06. This already occur at turbine 2, however, the discrepancy between the SUM method and the field data are relatively constant, ranging from 0.03-0.08, with the exception of turbine 4. The MAX and SQR method clearly overestimates the normalized wind speed, although this corrupted by the overestimation at turbine 2.

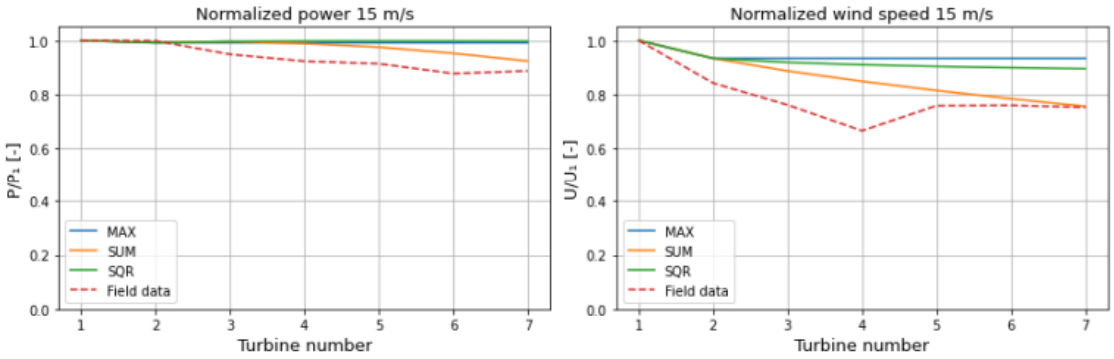

Figure 4.3: Normalized power and normalized wind speed at 15 m/s.

Figure 4.3 shows that the power production is slightly reduced by the rear end of the row. The field measurements shows a reduction of the normalized power production starting at turbine 3. The SUM method estimates that the power production is below rated from turbine 5. As it estimates a steeper and steeper reduction of power, the SUM method could most likely not provide good results in a row of more than eight turbines in a wind farm with such turbine turbine spacing. The MAX and SQR method estimates rated power for the whole row. However, a much larger difference is observed for the normalized wind speed. The difference between the simulations and the field data of the normalized wind speed is severe, starting at turbine 2, before the wake merging takes place. This difference is approximately 0.12, and even larger for turbine 3 and 4. Because of this difference in the front end of the row, the fine agreement seen from turbine 5-7 for the normalized wind speed becomes less interesting.

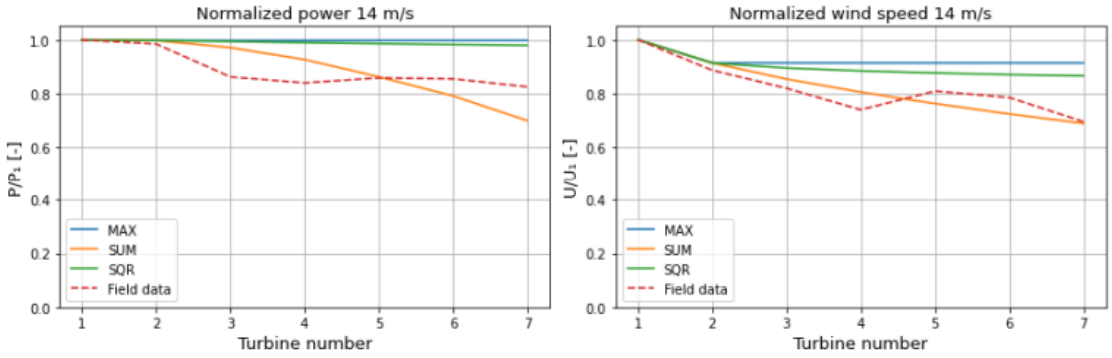

Figure 4.4: Normalized power and normalized wind speed at 14 m/s.

The power production at 14 m/s presented in figure 4.4 shows that the SUM method has the best agreement with the measurements, like the situations at 15-17 m/s. The model estimates the wake losses with high precision at turbine 2. Further, the SUM method estimates the wake losses with good accuracy further downstream for the normalized wind speed. At 14 m/s, wake losses are also clearly observed by investigating the normalized power production, as the turbines downstream of turbine 1 experience wind speeds below rated wind speed. As the result of this, this figure provides the best comparison between the different wake merging methods above rated wind speed. An interesting observation is that the SUM method behaves differently for the wind speed simulations and the power simulations, with accelerating decrease of the power, and a close to linear decrease for the normalized wind speed.

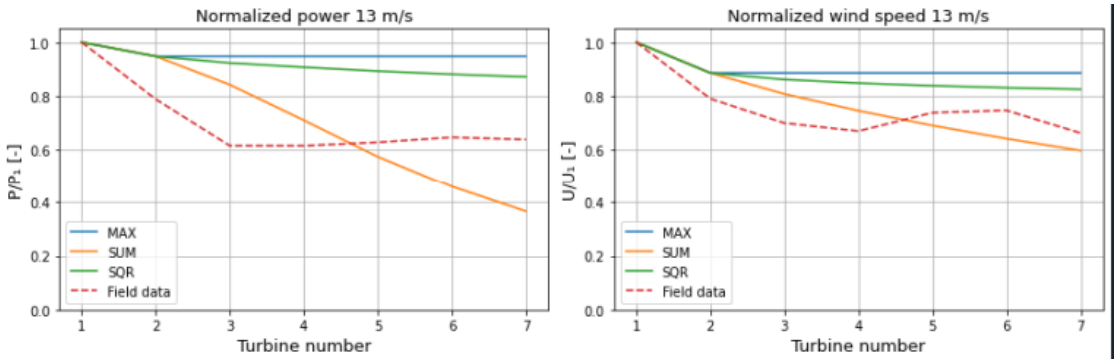

Figure 4.5: Normalized power and normalized wind speed at 13 m/s.

Figure shows a rather obscure result already at turbine 2, where there is a difference between the simulations and the field data of approximately 0.14 for the

normalized power production. For turbine 3, this difference is about 0.25. Thus, it is not meaningful to describe how the different wake merging methods performs compared to the field data further downstream at 13 m/s, which is the rated wind speed, as mentioned in chapter 3. However, the field data is of particular interest for this wind speed. The power production decreases linearly from turbine 1 to turbine 3, and is almost constant further downstream. This is a unique pattern compared to situations for the other wind speeds and is further discussed in chapter 5.

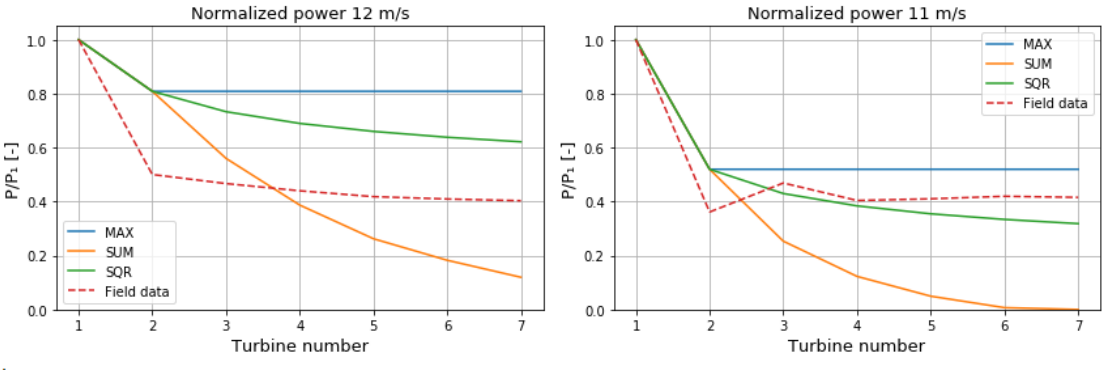

Figure 4.6: Normalized power at 12 and 11 m/s.

As seen in 4.6, there is a very large difference between the simulations and the field data already at turbine 2, approximately 0.3, before the wake merging procedure begins. With a difference this large, it is not meaningful describe the performance of the wake merging methods, like the situation at 13 m/s. This is further discussed in chapter 5. However, an interesting observation is that the normalized power production for turbine 2 is reduced from 0.94 at 13 m/s as seen in figure , to 0.81 at 12 m/s as seen in figure 4.6.

Nevertheless, the results are better at 11 m/s. Problems already occur at turbine 2 for this situation as well, where the discrepancy of the normalized power is approximately 0.16 at turbine 2 between the model and the field data, which corrupts the comparison between the wake merging methods in a large degree. However, the results should be further described. The discrepancy is reduced further downstream for the MAX method, and the power production slowly increases, where it is at maximum for turbine 3. The SQR shows a better agreement with the field data compared to the MAX method, but is a result of the overestimation at turbine 2. The normalized power is rather constant from turbine 4, thus, the MAX method shows best agreement with the field data at 11 m/s with an average overestimation of the normalized power production of approximately 0.12. An

interesting observation here is the large normalized power reduction for turbine 2 from 12 m/s to 11 m/s, which is approximately 0.28.

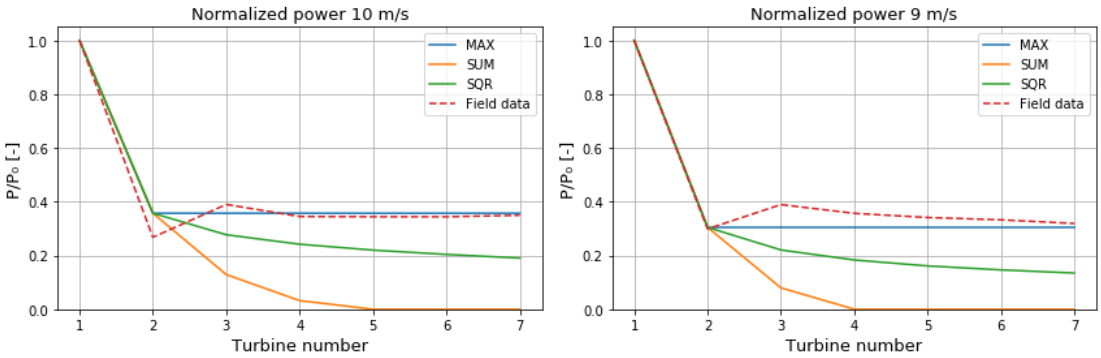

Figure 4.7: Normalized power at 9 and 10 m/s.

Shown by figure 4.7, the SUM method does not work at wind speeds significantly below rated wind speed, and neither does the SQR method. However, at 10 m/s, the MAX method shows a very fine agreement with the field data. Although it does not capture the deep deficit at turbine 2, nor the large wake recovery for turbine 3, a fine agreement is seen for the rear part of the row. At 10 m/s, the MAX method overpredicts the power production with 6%. At 9 m/s, the deficit for turbine 2 is captured accurately. As seen for the field data, the highest power production occur at turbine 3, with a slowly decreasing power production further downstream. For the rear part of the row, a small discrepancy is observed between the field data and the MAX method.

4.1.2 Row D

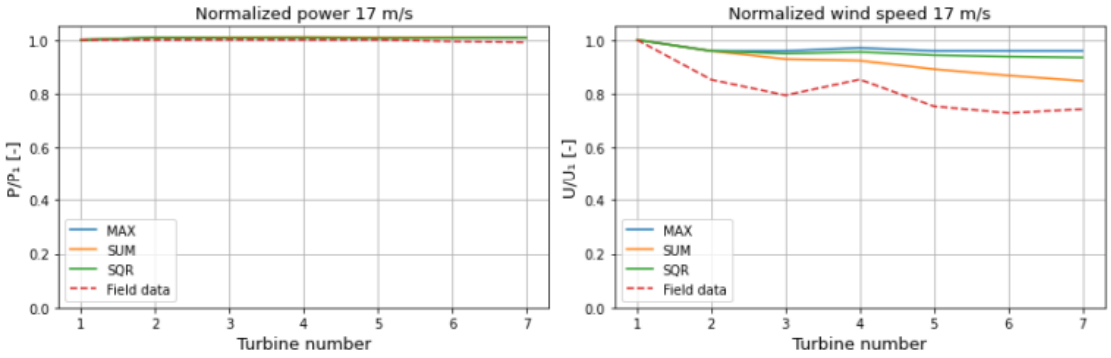

Figure 4.8: Normalized power and normalized wind speed at 17 m/s.

At 17 m/s, all the turbines in the row achieve rated power production, in agreement with the field data. However, as seen for the normalized wind speed in figure 4.8, the error already occur at turbine 2, as the situation for most of the cases in row C. The difference between the simulations and the field data is more than 0.10. However, the SUM method follows a similar pattern as the field data, although the wake recovery at turbine 4 is not captured.

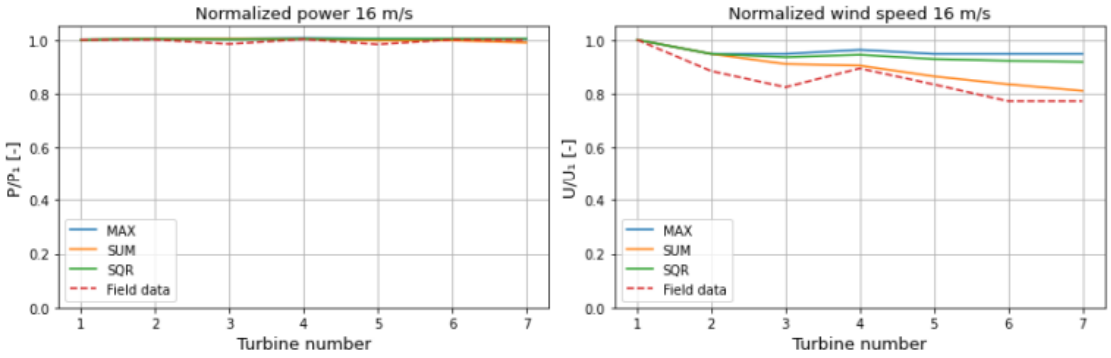

Figure 4.9: Normalized power and normalized wind speed at 16 m/s.

Figure 4.9 shows that the power production is constantly at rated power for all turbines in the row, like the situation at 17 m/s. Thus, the wake losses are better illustrated with the the wind speed. The model estimates a normalized wind speed around 0.95, with a difference of 0.06 already at turbine 2. However, the SUM method captures the tendency of a slowly linear reduction of the wind speed development, with an average overestimation of approximately 0.05.

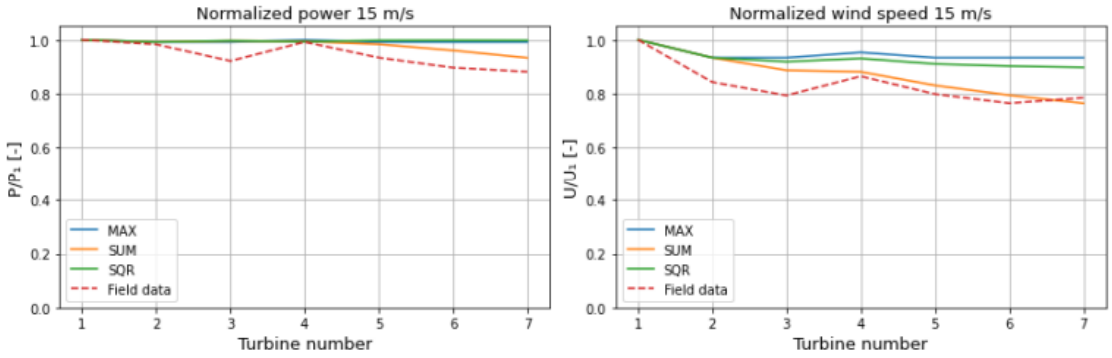

Figure 4.10: Normalized power and normalized wind speed at 15 m/s.

Figure 4.10 shows at fine agreement between the SUM method and the field data for the rear part of the row, when investigating the normalized wind speed, but does not capture the velocity deficit for the front part of the row. The measurements show that the power production is close to rated, approximately 90%, and full power production is reached for the fourth turbine. The fine agreement for the rear part of the row, which is observed in figure 4.8-4.11, is described in chapter 5.

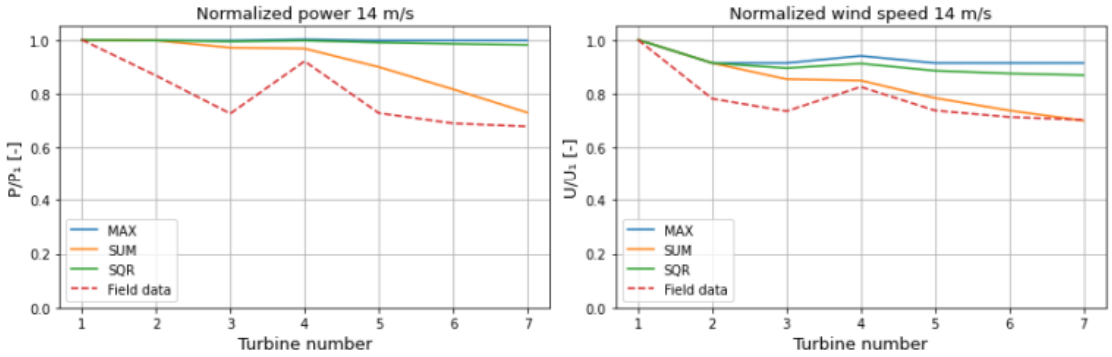

Figure 4.11: Normalized power and normalized wind speed at 14 m/s.

There is a very large discrepancy already at turbine 2 between the model and the field data, which affects the wake merging methods further downstream. The field data are quite different compared to the field data presented in figure 4.4, which also affect the comparisons between the model. Although the discrepancy between SUM method and the field data is not that bad for the normalized wind speed, the discrepancy is more than 0.20 at turbine 3, and around 0.17 for turbine 2. The MAX and SQR method estimates approximately rated power for all the turbines in the row.

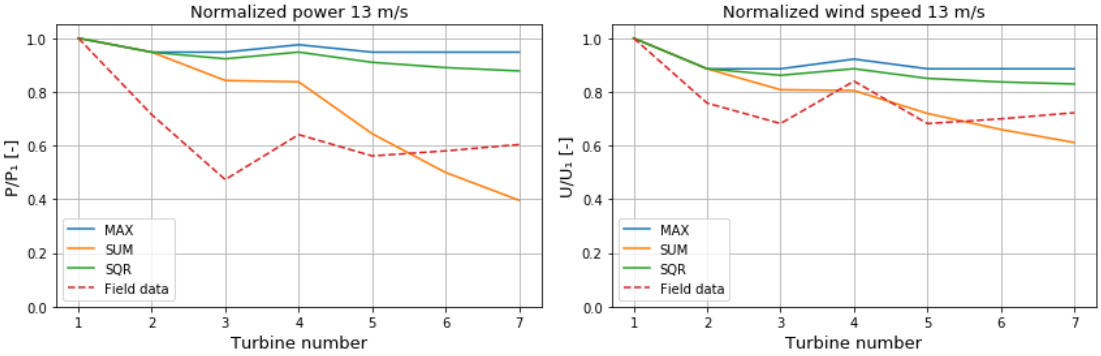

Figure 4.12: Normalized power and normalized wind speed at 13 m/s.

As seen in figure 4.12, the results at 13 m/s, which is the rated wind speed, is rather obscure. The field data shows a much deeper wake deficit than the simulations. There is a difference of 0.22 between the simulations and the field data already at turbine 2. This is even worse at turbine 3, where the difference for the normalized power production and the field data is more than 0.35. In other words, the SUM method estimates around 70% higher power production than the measurements. A further description of the results is thus meaningless. A similar pattern is seen for the normalized wind speed, although the discrepancy is less significant.

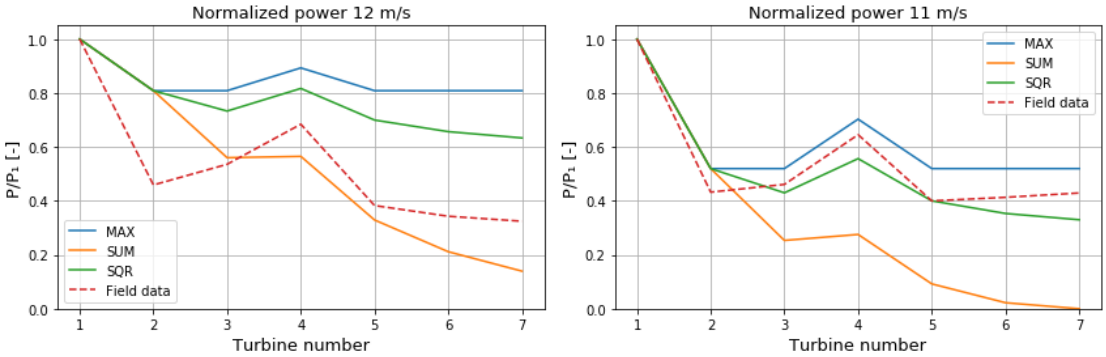

Figure 4.13: Normalized power at 11 and 12 m/s.

For figure 4.13, the normalized power production at 12 m/s and 11 m/s is shown. The difference of the normalized power production between the simulations and the measurements is more than 30% for turbine 2 at 12 m/s. With a difference this large already at turbine 2, it is meaningless to compare the wake merging methods any further for this particular case. It should also be pointed out that the measured wake loss observed for the rear end of the turbine is rather strange.

By investigating the field data for the normalized power in row D, the normalized power production gradually decreases with decreasing wind speed. However, there is an exception at 12 m/s, where the normalized power is lower in the rear end of the row compared to the situation at 11 m/s and 10 m/s, as seen in figure 4.14.

At 11 m/s, a much better agreement between is observed. The normalized power production is 0.09 higher for the simulations compared to the field data at turbine 2. For turbine 3 and 4, this is approximately 0.06 with the MAX method, corresponding to 12% higher power production. For the rear of the row, the difference is a 0.10-0.12 for the MAX method. The SUM method is clearly overestimating the wake losses. However, the SQR method does also perform quite well for this wind speed. Although it does not follow the pattern of the field data in the same way as the MAX method, and underestimates the power production for most of the turbines, this method shows in average better results than the MAX method. However, this is a result of the discrepancy which already occur at turbine 2. These results are also in agreement with the results from figure 4.6, where the MAX and SQR method show similar results at 11 m/s.

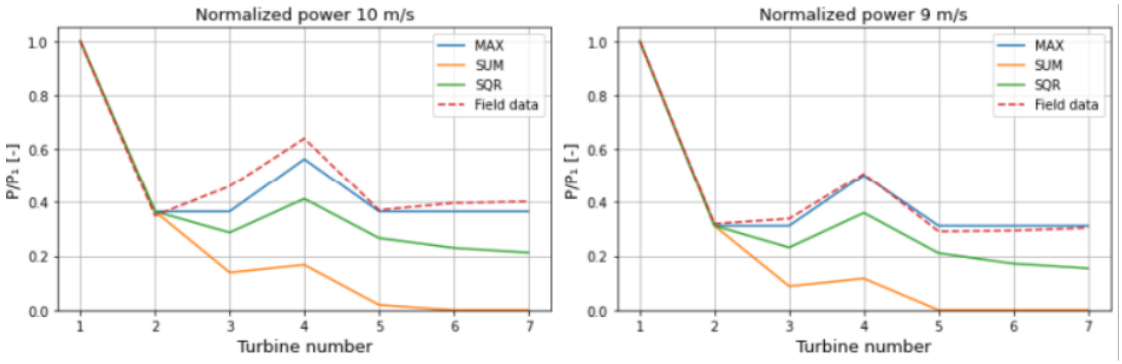

Figure 4.14: Normalized power at 9 and 10 m/s.

At 9m/s and 10 m/s shown in 4.14, the model estimates the wake loss between turbine 1 and 2 accurately for both wind speeds. It is clearly observed that the SQR method and the SUM method do not work at wind speeds this low. At 9 m/s, the SUM method even calculates negative wind speeds. The MAX method do not capture the wake recovery between turbine 2 and 3 at 10 m/s, and thus, it underestimates the wake recovery for the large turbine spacing between turbine 3 and 4. There is a better agreement for the rear part of the row between the field data and max method. The max method underestimates the power production with an average of 11% at 10 m/s.

At 9 m/s, a very fine agreement between the MAX method and the field data is observed. The difference of the predicted normalized power production for the

MAX method and the field data is in the order of 0.02. Thus, the max method underestimates the power production with an average 4% for the front part of the row. For the rear part of the row, the MAX method underestimates power production with 5%.

4.2 Radial wake deficit

This section was partly covered in chapter 3, where figure 3.3 shows the development of the radial single wake deficits in a row of seven turbines. However, since the power production is investigated for a range of nine wind speeds wind speeds, the development of the wake in the radial direction of some of these wind speeds is of interest.

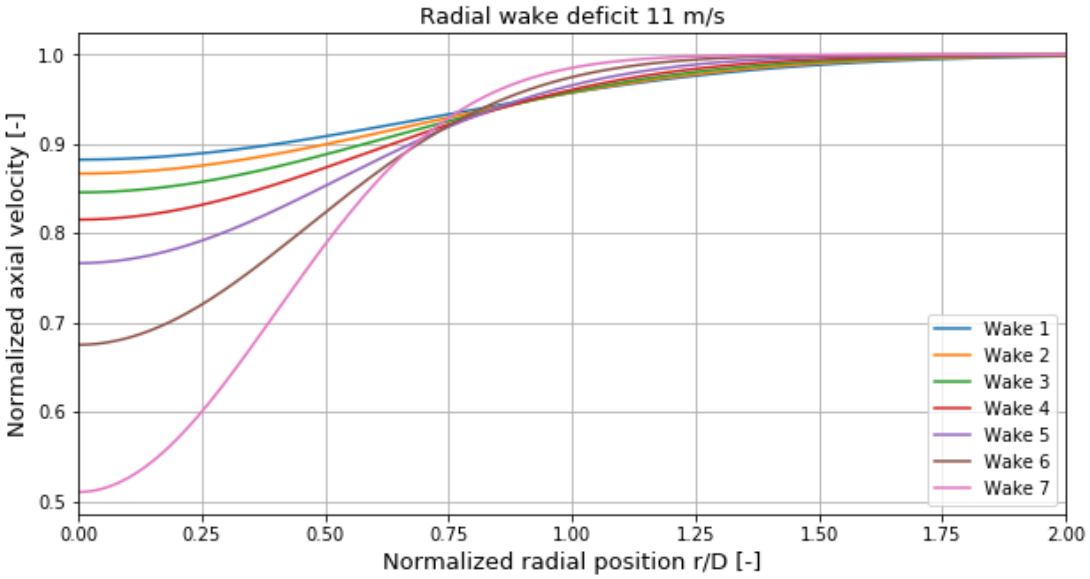

Figure 4.15: Radial wake deficit at 11 m/s, seen from a position of 4.3D behind the seventh turbine, in a row with seven turbines and a turbine spacing of 4.3D.

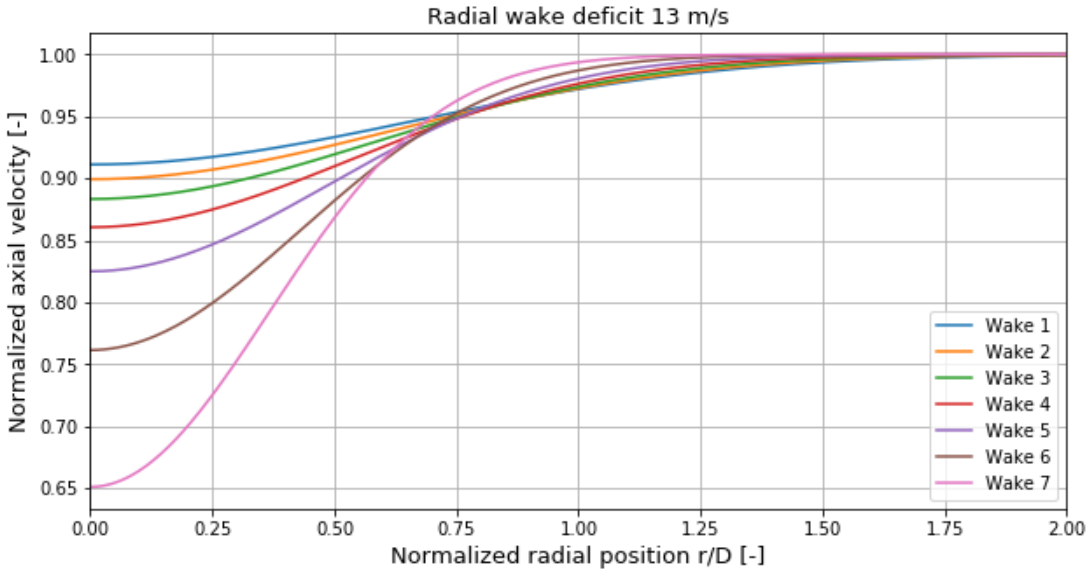

Figure 4.16: Radial wake deficit at 13 m/s, seen from a position of 4.3 diameters behind the seventh turbine, in a row with seven turbines and a turbine spacing of 4.3D.

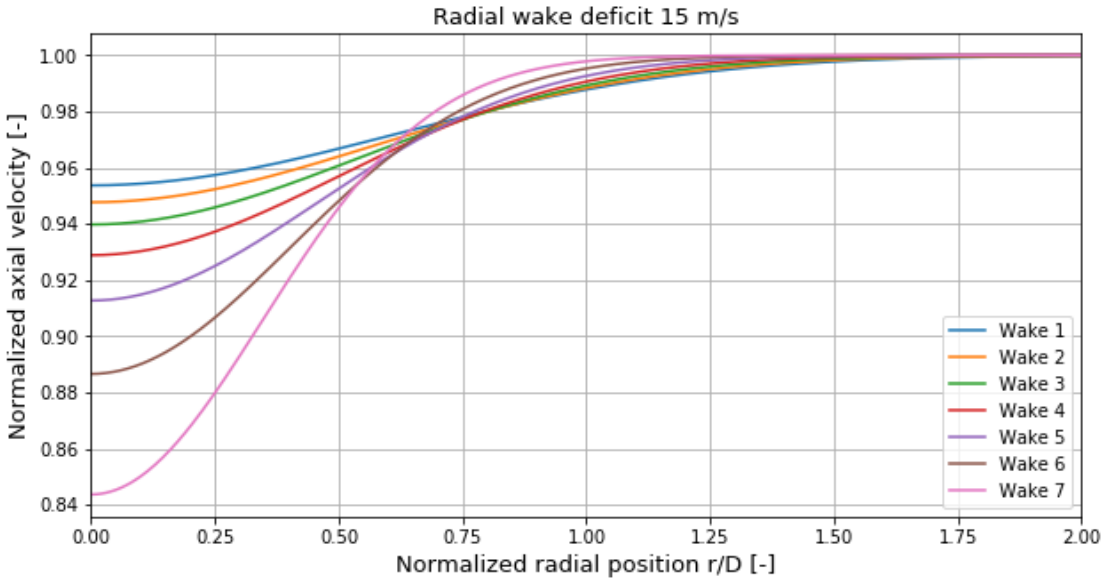

Figure 4.17: Radial wake deficit at 15 m/s, seen from a position of 4.3 D behind the seventh turbine, in a row with seven turbines and a turbine spacing of 4.3D.

From figure 4.15-4.17, it is seen that wake from the seventh turbine is the domin-

ating wake for all the cases. This in agreement with figure 3.3. Furthermore, the single wake loss from each turbine is decreasing with increasing wind speeds. It is also seen that the wake from turbine 1 is the dominating wake after a distance of about 0.85 r/D for the at 11 m/s shown in figure 4.15, and a distance of 0.75 r/D. Thus, the wake from the last turbine in the row start to dominate earlier in the radial position, with increasing wind speeds.

4.3 Velocity profile

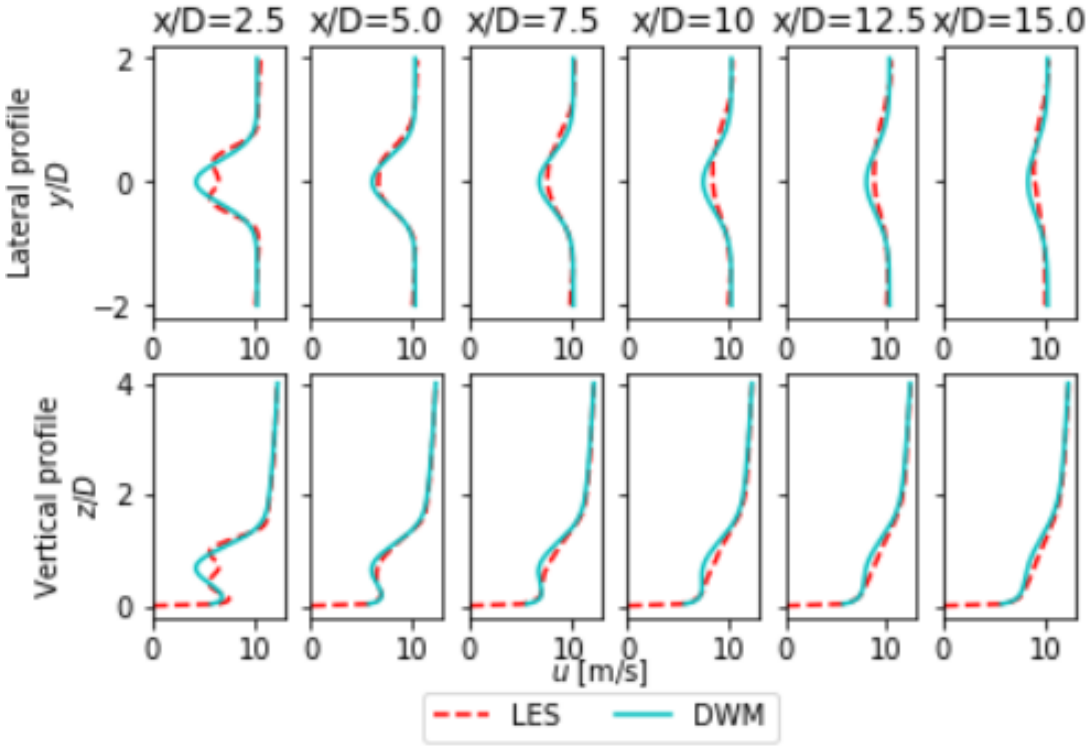

Figure 4.18: Axial velocity profile in lateral and vertical directions

Figure 4.18 shows the development of the axial velocity in lateral and vertical direction for the 5MW NREL turbine, where the DWM model is compared with LES simulations. The velocity profile of the DWM model is not defined at $z = 0$, which results in the difference between the DWM model and the LES simulations, seen from 0 m/s to about 5 m/s for the vertical profile. As observed in the figure,

there is a significant development between 2.5D and 5.0 D. This is discussed further in chapter 5.

Chapter 5

Discussion

5.1 Field data

As seen from the results in chapter 4, it is not always the case that a clear pattern can be observed for the field data, by comparing the results at various wind speeds. It is for instant measured a lower wake loss at 16 m/s for row C, seen in figure 4.2, compared to the case at 17 m/s seen in figure 4.1, and the case at 15 m/s, seen in figure 4.3. The same is observed in figure 4.8-4.10 for row D. Even though the measurements are gathered over a time period of eight months, there were only a few measurements for each case above rated wind speed which could be obtained within the required bin angle. Nevertheless, the number of measurements at high wind speeds are considered to be sufficient enough, although this gives high uncertainties. This is the reason for the choice of having a larger bin angle for the downstream turbines in a row, than the upstream turbines.

A choice of 2.0° bin angle is rather small, but gives a more precise range of wind inflow angles for the simulated cases. The length of the rows is approximately 2.5 km as seen in figure 3.1, and the wind direction is in most cases not exactly constant of such distances. In the order to obtain a sufficient amount of measurements at high wind speeds, a bin angle of 6.0° were accepted for the downstream turbines, as mentioned in chapter 3. A bin angle of 2.0° could have been accepted for lower wind speeds, as Keck [19] and Hao [51] compared simulations with field data from row B and D in Lillgrund for the whole row, with a bin angle of this order. Moreover, as mentioned in chapter 3, this bin angle is the reason why row C is simulated with seven turbines instead of eight. There were simply not enough

measurements for turbine C1 at several wind speeds around rated. Thus, this turbine was excluded from the simulations. A solution for this could have been to implement wind speeds within a bin angle of 6.0° for the first turbine in each row, which would have provided a higher number of measurements, reducing the uncertainty of having few measurements for certain wind speeds, although, several of these measurements would not be aligned with the row.

As mentioned in chapter 3, measurements from the meteorological mast could not be obtained, and as a consequence of this, the field data are not filtered based on the atmospheric stability. This is a major source of uncertainty when comparing the measurements with the field data, as the cases are simulated with a neutral stability class. However, as mentioned in the theory, previous studies state that the power estimation under neutral stratification is between the power estimation for stable and unstable stratification. Thus, the field data can be considered to be averaged, and approximate neutral stratification to some degree. Moreover, it were observed different power production at the same wind speeds for some of the measurements, from the same turbines. The reason for this could be a calibration issue for the anemometers of the individual turbines. This issue demonstrates the importance of enough measurements to average, and the vulnerability of having few measurements above rated wind speed.

5.2 Power production

As seen in figure 4.1-4.5 by investigating the normalized wind speeds, there is a significant wake loss for turbine C5 and C2, compared to the rest of the turbines in the row for the normalized wind speeds. This is turbine number 4 and turbine number 7, seen in the figures of row C, figure 4.1-4-7. This wake loss is not observed for the power production in figure 4.4 and 4.5, which indicates there is a small calibration error for the anemometers belonging to turbine C5 and C2. If there is in fact a calibration issue with the anemometers of these turbines, and the anemometers measures too low wind speeds, the SUM method estimates the wake losses better than figure 4.1-4.5 actually show. These results are in agreement with Barthelmie et al. [26], stating that the wake losses for high wind speeds is much smaller compared to the wake losses for lower wind speeds.

As observed by figure 4.5 and 4.6, this version of the DWM model is not able to predict wake losses around rated wind speed. This is in agreement with the results from Larsen et al. [20]. The same is observed in figure 4.12 and 4.13, at 13 m/s and 12 m/s for row D. Based on these results, a different wake merging approach

is needed for the wind regime around rated wind speed, but most important, the velocity at turbine 2 must be modelled correctly before the wake merging procedure begins, which is further discussed below.

The sequential approach suggested by Madsen et al. [76], gives a better estimate at 12 m/s. However, the DWM model is not used in that paper, and the sequential approach does not include wake meandering. This means it is not straightforward to include this summation method in the DWM model. In this paper, the measured normalized power is approximately 0.65 for turbine 2, while the measured normalized power for turbine 2 in this study is 0.50 for row C as seen in figure 4.6, and 0.48 for row D, as seen in figure 4.13. It is not clear whether the measurements presented in [76] are from row B or C in Lillgrund, and the stability class is not specified. Nevertheless, this difference illustrates uncertainties for the field data.

Nevertheless, the main problem with the simulations in this thesis, which is observed in most of the figures for wind speeds ranging from 11-17 m/s, is estimating the wake loss accurately between turbine 1 and 2. As observed in figure 4.5, 4.6, 4.12 and 4.13, there is a very large discrepancy around rated, at 12 m/s and 13 m/s respectively, but also at 14 m/s for row D, as seen in figure 4.11. Since this is before the wake merging procedure begins, this is a result of the velocity deficit model. As mentioned in chapter two, the largest wake losses occur at wind speeds well below rated, where the thrust coefficients are high, and the lowest occur at high wind speeds. As seen in figure 3.2, the thrust coefficient is reduced from 0.79 at 10 m/s, to 0.34 at 13 m/s, and this rapid change is one of the reasons why the estimation of the wake losses in this region is difficult.

Mentioned in chapter 4, and seen in figure 4.5 and 4.6, but also figure 4.12 and 4.13, the model estimates a normalized power at 13 m/s of 0.94, which drops down to 0.81 at 12 m/s. However, the model estimates a normalized power of 0.53 at 11 m/s. Furthermore, the normalized power at 10 m/s is 0.37. The drop between 12 m/s and 11 m/s is very large compared to the other situations, and indicates that the model is very sensitive in this velocity range. This is demonstrated with a small calculation example. For the situation at turbine 1 at 12 m/s, C_P=0.309 and C_T=0.437. For turbine 12, the velocity is 10.1 m/s, with C_P=0.419 and C_T=0.418. If velocity reduction to 9.5 m/s is assumed, which is a reduction of 6%, the thrust and power coefficient stay almost the same, where C_P=0.432 and C_T = 0.829. However, as the increases cubicly as a function of velocity, this reduced velocity has rather large influence of the power. For a velocity of 9.5 m/, the normalized power is reduced from 0.81 to 0.70. This demonstrates that correct modelling of the velocity is very important.

From the measurements, the velocity deficit ranges from approximately from 1.5-3.0 m/s, for wind speeds of 17-9 m/s at turbine 1. However, the velocity deficit varies with 0.8-3.0 for the simulations. Estimating this deficit correctly will improve the results significantly around and above rated.

The fact the velocity for turbine 2 is calculated at the turbine position, could cause a small error. A different approach is to calculate this velocity upstream of turbine 2, for example 1D from the rotor. This has been checked for velocities ranging from 9-13 m/s. At 13 m/s, the normalized power was reduced from 0.94 to 0.93, thus, only a very small reduction. For 12 m/s, the velocity was reduced with 0.2 m/s, from 10.1 m/s to 9.9 m/s, reducing the normalized power from 0.81 to 0.775. At 9 m/s, the normalized power is reduced from 0.31-0.25. This illustrates that changing the position of where the reference velocity is calculated for the turbines only have small impact on the power production at rated, and will be even smaller above rated. However, this approach have rather large influence well below rated, leading to an overestimation of the wake losses.

Although significant problems occur already at the second turbine, corrupting the comparisons between the wake merging methods, the pattern for the different wake merging methods should still be discussed for the situations at 12 m/s and 13 m/s. The rather linear wake loss down to turbine 3 is interesting, as observed in figure 4.5. However, if a fine agreement is assumed between the field data and simulations at turbine 2, none of the wake merging methods are able to capture the further linear decrease to turbine 3. This linear decrease from turbine 2 to turbine 3, with a rather constant power development further downstream, illustrates why power prediction around rated wind speed is difficult to predict accurately. The SUM method would have estimated the power with good accuracy for turbine 3, but calculated way too large deficit further downstream. The MAX method would estimate the same power production further downstream, as calculated for the second turbine. Hence, the SQR method would most likely given the best result at 13 m/s for row C, assuming that difference in the power production for turbine 2 and 7 would been around 0.08.

However, comparing the SQR method and the field data at 12 m/s for row C, is interesting. With accurate modeling for turbine 2, the SQR method could potentially the wake development with good accuracy for this wind speed, are there is a the pattern between the SQR method and the field data is quite similar, with a squared reduction of the power production. The results at 12-14 m/s is even worse in row D. The field data are even lower for turbine 2 and 3, as observed in figure 4.11 and 4.12, which could be a result of variable atmospheric stabily, different turbulence intensity, variation of inflow angle and calibration issues. In

theory, the field data for turbine 1-3 should be equal for the two rows. This holds for most of the cases, although there are always some small exceptions, and quite significant at 12 and 13 m/s.

The fine agreement observed between the SUM method and the field data for the rear part of row D at wind speeds above rated, seen in figure 4.8-4.10, is a result of the large turbine spacing turbine 3 and 4, which leads to a recovery of the wake, and reduces the wake losses. Thus, this is not a result of the wake merging method, as the SUM method do not capture this effect.

A shortcoming in the modelling of the wake development, to keep it purely axisymmetric, is the fact that only hub height wind speed is used as reference velocity. The effect of wind shear is thus ignored. Averaging the sheared profile over the first turbine, could give a slightly different velocity and the reference velocity used in the modelling. A small change in this velocity could result in a significant change of the power production.

This leads to the simulations conducted at 9 and 10 m/s, which shows that the MAX method is superior to the two other wind speeds for wind speeds well below rated. This quite expected, and in good agreement with the fact that it is implemented in the IEC standard [21]. Nevertheless, a weakness with this method the way it only estimates constant turbine production. The method does not capture the wake evolution properly, unless there is a rather constant power production downstream of the second turbine.

Keck [19] conducted a similar simulation as presented in figure 4.7 and 4.14 at 9 m/s for Lillgrund wind farm. His version of the DWM model captures the deep deficit, with an increasing power production for turbine 3. This is achieved by calculating the average axisymmetric velocity field at the downstream rotor over annular radial sections, and more correct way of calculating the wake deficit. However, this wake merging method is also way more time consuming, which is a clear disadvantage.

The deficits calculated with the SUM method at the lowest wind speeds are way too strong, and gives wind speeds around 0 m/s, which is a highly nonphysical result. This already occurs at 11 m/s. Based on the results shown in figure 4.6, 4.7, 4.13 and 4.14, there is no purpose to use the SUM method for wind speeds below 12 m/s in Lillgrund. Expressed more generally, SUM method should not be used for wind speeds below approximately 90% of the rated wind speed. However, with only two rows simulated in only one wind farm, there is not enough data to conclude with this, although the simulations gives a clear indication of the lower

limit where the SUM method is usable.

As seen for in the results, particularly for low wind speeds, the wake losses in Lillgrund are severe due to the tight turbine spacing. It is clearly observed for the field data, both in row C and D for wind speeds 9-11 m/s that the largest wake loss occur for at the second turbine, and a wake recovery for turbine 3. F. This is a result of increased turbulence behind the second turbine, which results in an increasing mixing in wake shear layer. With a turbine spacing of only 4.3D, the turbines are located in the intermediate wake of the turbine upstream, as illustrated by figure 2.5. As illustrated by figure 4.18, the wake develops severely between 2.5D and 5.0D. This is in agreement with the results presented by Hao [51] from Lillgrund and Egmond aan Zee. The wake recovery observed in row D after turbine 3 because of the increased turbine spacing, with a distance of 8.6D. This is in the far wake region, where the wake shear layer has fully expanded. The wake also expands and becoming shallower, resulting in an increased wind speed for turbine 4. The wind speed is in fact 1 m/s higher for turbine 4 compared to the rest of the downstream turbines in row D due to this gab, resulting in a normalized power from 0.31 to 0.50.

An interesting topic is the deep array effect. If the deep array effect occurs, the wake losses in the rear part of row should have been higher than the wake losses closer front part of the row, as these are exposed to more overlapping wakes. At 9 m/s and 12 m/s for row C, this is the case for row C. However, the investigated rows do not contain enough turbines to conclude whether or not the deep array effect exists. Furthermore, as mentioned previously, there are also uncertainties with the measurements, and it can not be concluded whether the deep array effect exist in this wind farm.

5.3 Velocity field and turbulence build-up

A clear weakness in this thesis is the modelling of the quasi-steady velocity deficit and the turbulence build-up, as blade data from the SWT-2.3-93 could not be obtained. Explained in the theory, an approach more similar to the one proposed by Ainslie [14], and further developed by Waldl [69] and Lange [68] is proposed. Also explained in the theory, this is not based on BEM theory, which gives two disadvantages. The velocity build-up and the wake expansion is modelled based on analytical gaussian expressions, which do not take the shape of the turbine blades into account and thus, properties like lift and drag are not calculated.. Thus, the modelling of the near and far wake is modelled by other equations, described in

Madsen et al. [17].

Furthermore, the major consequence of not having an approach based on BEM is a weaker implementation of the turbulence build-up. BEM theory is important for the implementation of the updated turbulence formulation of the DWM model presented by Keck [19]. Even though the implementation of the eddy viscosity used in this thesis captures the effect from the the ambient turbulence and the self-generated turbulence, a complete version of the wake added turbulence is not implemented in this version of the DWM model. The increased power production Keck estimated, by implementing an updated turbulence formulation, indicates that this version of the DWM model underestimates the power production with a few percent compared to an updated version based on BEM theory and a complete turbulence formulation. This hypothesis is in fine agreement by comparing the results from [19] [51], where each respective version of DWM model estimates lower wake losses at 9 m/s. However, the results from Lillgrund in this study at 9 m/s and 10 m/s are satisfactory. Nevertheless, the bin angle used in this thesis is not the same as the bin angle used in [19] and [51], which affects the comparisons. The uncertainty for the atmospheric stability will of course also affect the result. It would be interesting to investigate whether or not the results are improved around and above rated wind speed, if BEM theory and a complete turbulence formulation is implemented in the model.

Chapter 6

Conclusion

6.1 Lillgrund offshore wind farm

The power production for wind speeds ranging from 9-17 m/s has been investigated in this study. The main goal was to estimate the power production around and above rated wind speeds. This was conducted by using three different methods for wake merging, denoted MAX, SQR and SUM, and comparing the simulations with field measurements for the various wind speeds, for two different rows in Lillgrund offshore wind farm.

From these simulations, it is clear that two merging methods are suitable for power estimation in different ranges of the wind speed. The MAX method superior to the two other well below rated wind speed, preferably at 9 m/s and 10 m/s in Lillgrund. The SUM method shows better results than the two other methods around and above rated wind speed, from 14 - 17 m/s. However, none of the methods provides an acceptable estimation of the power production for wind speeds around rated wind speed. This yields particularly at 12 m/s and 13 m/s, where the latter is the rated wind speed in Lillgrund. However, the under prediction of the wake losses already at turbine 2, obscures the comparisons between wake merging methods to some degree, where this discrepancy is very significant at 12 m/s and 13 m/s. This also affect the results above rated wind speed. However, it is concluded that the MAX is suited for power estimation well below rated wind speed, and the SUM method is suited for power estimation above rated wind speed, in agreement with the IEC standard. Results at 12 m/s 13 m/s indicates that the SQR could be used for estimation of the wake losses at those wind speeds, although with low accuracy,

but more accurate modelling of the velocity deficit is needed, before this can be tested properly.

6.2 Further work

There are in general three ways to improve the power prediction around rated wind speed. The first is to improve the wake model, so the wake losses are calculated accurately for the various wind speeds at turbine 2. This very important, as the results around rated wind speed will be significantly improved. Furthermore, this will also improve the ability of estimating wake losses above rated wind speed. The second is to develop a completely new method to estimate the wake losses around rated wind speed. If this occur in the future, a major issue is resolved in wind energy engineering. The third is to test other, already developed wake merging methods. The wake merging methods suggested by Keck **Keck** and by Zong and Porté-Agel [77] are promising, but these methods are not yet tested for power prediction around and above rated wind speed. An issue with the first method is computational time, and the second was developed very recently, and has not yet been tested in the DWM model. Nevertheless, it would be interesting to see how these methods perform around rated wind speed. Furthermore, as mentioned in chapter 2 and 5, this version of the DWM model is not based on a BEM approach, as blade data for the turbines in Lillgrund not could be obtained. The wake merging methods used in this thesis should therefore be used in a version similar to the complete DWM formulation proposed by Keck [19], for further validation of these wake merging methods, and the wake model used in this thesis.

There are also a couple of other research topics which would be interesting to investigate with DWM model:

(1) Multiple wake situations for non-aligned flow cases: The evolution of the wake deficit implemented in the DWM model is modelled with an axisymmetric deficit approach. This limits the possibility to include situations where the inflow is not aligned with the turbine row. Furthermore, cases with lateral wake merging, which may occur deep inside the wind farm or for neighbouring rows with very narrow spacing in the lateral direction, would also be interesting to include in the DWM model. Thus, the wake effects of a complete wind farm could be captured with one single simulation.

(2) Deep array effect: The deep array effect should be investigated with the DWM model in very large wind farms. This is important for layout purposes

Bibliography

[1] United Nations, 'Paris agreement', p. 16, 2015, Accessed: 2020-04-11. [Online]. Available: https://unfccc.int/files/meetings/paris_nov_2015/application/pdf/paris_agreement_english_.pdf.

[2] Wind Europe, 'Floating offshore wind energy, A policy blueprint for europe', 2018, Accessed: 2020-08-11. [Online]. Available: https://windeurope.org/wp-content/uploads/files/policy/position-papers/Floating-offshore-wind-energy-a-policy-blueprint-for-Europe.pdf.

[3] Global Wind Energy Counsil, 'Gwec - global wind report 2019', 2020, Accessed: 2020-08-10. [Online]. Available: https://gwec.net/.

[4] *World wind capacity at 650,8 gw, corona crisis will slow down markets in 2020, renewables to be core of economic stimulus programmes*, Accessed: 2020-08-10. [Online]. Available: https://wwindea.org/blog/2020/04/16/world-wind-capacity-at-650-gw/.

[5] ——, 'Global offshore wind report 2019', 2020, Accessed: 2020-08-11. [Online]. Available: https://gwec.net/wp-content/uploads/dlm_uploads/2020/08/GWEC-offshore-wind-2020-5.pdf.

[6] BloombergNEF, *New energy outlook 2019*, Accessed: 2020-08-11. [Online]. Available: https://wwindea.org/blog/2020/04/16/world-wind-capacity-at-650-gw/.

[7] Global Wind Energy Counsil, 'Gwec - global wind report 2018', 2019, Accessed: 2020-08-11. [Online]. Available: https://gwec.net/wp-content/uploads/2020/02/Annual-Wind-Report_digital_full-1.pdf.

[8] Wind Europe, 'Wind energy in europe in 2019, Trends and statistics', 2020, Accessed: 2020-08-11. [Online]. Available: https://windeurope.org/wp-content/uploads/files/about-wind/statistics/WindEurope-Annual-Statistics-2019.pdf.

[9] International Renewable Energy Agency, 'Renewable power generation costs in 2018', 2019, Accessed: 2020-08-11. [Online]. Available: https://www.irena.org/-/media/Files/IRENA/Agency/Publication/2019/May/IRENA_Renewable-Power-Generations-Costs-in-2018.pdf.

[10] P. B. S. Lissaman, 'Energy effectiveness of arbitrary arrays of wind turbines', 1979. DOI: 10.2514/6.1979-114.

[11] P. E. J. Vermeulen, 'An experimental analysis of wind turbine wakes', in *3rd International Symposium on Wind Energy Systems*, 1980, pp. 431–450.

[12] J. F. Ainslie, 'Development of an eddy viscosity model for wind turbine wakes', 1985.

[13] S. N. W. Robert W. Baker, 'Wake measurements behind a large horizontal axis wind turbine generator', *Solar Energy 33(1):5–12*, 1984. DOI: 10.1016/0038-092X(84)90110-5.

[14] J. F. Ainslie, 'Calculating the flowfield in the wake of wind turbines', *Journal of Wind Engineering and Industrial Aerodynamics*, 1988.

[15] H. Aagaard Madsen, K. Thomsen and G. Larsen, 'A new method for prediction of detailed wale loads', English, IEA Annex XI Joint Action Meeting 16 on "Aerodynamics of Wind Turbines" ; Conference date: 05-05-2003 Through 06-05-2003, 2003.

[16] G. Larsen, H. Madsen, K. Thomsen and T. Larsen, 'Wake meandering: A pragmatic approach', *Wind Energy*, vol. 11, pp. 377 –395, Jul. 2008. DOI: 10.1002/we.267.

[17] H. Aagard Madsen, G. Larsen, T. Larsen, N. Troldborg and R. Mikkelsen, English, *Journal of Solar Energy Engineering*, vol. 132, no. 4, 41014 (14 pages), 2010, ISSN: 1999-231. DOI: 0.1115/1.4002555.

[18] T. Larsen, H. Aagaard Madsen, G. Larsen and K. Hansen, English, *605–624*, vol. 16, no. 4, pp. 605–624, 2013, ISSN: 1095-4244. DOI: 10.1002/we.1563.

[19] R. E. Keck, D. Veldkamp, J. J. Wedel-Heinen and J. Forsberg, 'A consistent turbulence formulation for the dynamic wake meandering model in the atmospheric boundary layer', English, PhD thesis, Denmark, 2013.

[20] T. Larsen, G. Larsen, H. Aagaard Madsen and S. Petersen, 'Wake effects above rated wind speed. an overlooked contributor to high loads in wind farms', English, in *Scientific Proceedings. EWEA Annual Conference and Exhibition 2015*, European Wind Energy Association (EWEA), 2015, pp. 95–99, ISBN: 9782930670003.

[21] IEC 61400-1:2019 edition 4, 'Wind energy generation systems - part 1: Design requirements', International Electrotechnical Commission, International Standard, 2019.

[22] P.-E. Réthoré, P. Fuglsang, T. Larsen, T. Buhl and G. Larsen, *TOPFARM wind farm optimization tool*, English, ser. Denmark. Forskningscenter Risoe. Risoe-R 1768(EN). Risø National Laboratory for Sustainable Energy, Technical University of Denmark, 2011.

[23] J. F. Manwell, J. McGowan and R. A.L., *Wind Energy Explained, Theory, Design and Application*, Second. John Wiley and Sons, Ltd, 2009.

[24] T. Burton, D. Sharpe, N. Jenkins and E. Bossanyi, *Wind energy handbook*. John Wiley Sons, Ltd., 2011.

[25] K. S. Hansen, R. J. Barthelmie, L. E. Jensen and A. Sommer, 'The impact of turbulence intensity and atmospheric stability on power decits due to wind turbine wakes at horns rev wind farm', *Wind Energy*, vol. 15, pp. 183–196, 2012. DOI: 10.1002/we.512.

[26] R. J. Barthelmie, K. S. Hansen and S. C. Pryor, 'Meteorological controls on wind turbine wakes', *Proceedings of the IEEE*, vol. 101, no. 4, 2013. DOI: 10.1109/JPROC.2012.2204029.

[27] B. Sanderse, 'Aerodynamics of wind turbine wakes, Literature review', 2009.

[28] D. L. Elliott, 'Status of wake and array loss research', 1991.

[29] N. Cetin, M. A. Yurdusev, R. Ata and Aydoğan, 'Assessment of optimum tip speed ratio of wind turbines', *Mathematical and Computational Applications*, vol. 10, no. 1, pp. 147–154, 2015. DOI: 10.3390/mca10010147.

[30] E. Dupont, R. Koppelaar and H. Jeanmart, 'Global available wind energy with physical and energy return on investment constraints', *Applied Energy*, 2017. DOI: 10.1016/j.apenergy.2017.09.085.

[31] R. Barry and R. J. Chorley, *Atmosphere, Wheather and Climate*, Ninth Edition. Routledge, 2010.

[32] A. Obukhov, 'Turbulence in an atmosphere with a non-uniform temperature', English, *Probabilistic Engineering Mechanics*, pp. 7–29, 1971.

[33] A. S. Monin and A. Obukhov, 'Basic laws of turbulent mixing in the surface layer of the atmosphere', English, vol. 151, pp. 163–187, 1954.

[34] A. M. Sempreviva, R. J. Barthelmie and S. C. Pryor, 'Review of methodologies for offshore wind resource assessment in european seas', *Surveys in Geophysics*, vol. 6, no. 29, pp. 471–497, 2008. DOI: 10.1007/s10712-008-9050-2.

[35] T. Foken, *Micrometeorology*, second. Springer, 2017, ISBN: 978-3-642-25439-0. DOI: 10.1007/978-3-642-25440-6.

[36] A. Peña, S.-E. Gryning and J. Mann, 'On the length-scale of the wind profile', *Quarterly Journal of the Royal Meteorological Society*, vol. 136, no. 653, pp. 2119–2131, 2010. DOI: 10.1002/qj.714.

[37] B. R. J., 'The effects of atmospheric stability on coastal wind climates', *Meteorological Applications*, vol. 6, no. 1, pp. 39–47, 1999. DOI: 10.1017/S1350482799000961.

[38] R. J. Barthelmie and L. E. Jensen, 'Evaluation of wind farm efficiency and wind turbine wakes at the nysted offshore wind farm', *Wind Energy*, vol. 13, no. 6, pp. 573–586, 2010. DOI: 10.1002/we.408.

[39] S. Wharton and J. K. Lundquist, 'Assessing atmospheric stability and its impacts on rotor-disk wind characteristics at an onshore windfarm', *Wind Energy*, vol. 15, no. 4, pp. 525–546, 2012. DOI: 10.1002/we.483.

[40] R. J. Barthelmie, S. Frandsen, S. Nielsen, S. Pryor, P. Réthoré and H. Jørgensen, 'Modeling and measurements of power losses and turbulence intensity in wind turbine wakes at middelgrunden offshore wind farm', *Wind Energy*, vol. 10, pp. 517–528, 2007. DOI: 10.1002/we.

[41] L. Alblas, W. Bierbooms and D. Veldkamp, 'Power output of offshore wind farms in relation to atmospheric stability', *Journal of Physics: Conference Series*, vol. 555, 2014. DOI: 10.1088/1742-6596/555/1/012004.

[42] A. Sathe and W. Bierbooms, 'Influence of different wind profiles due to varying atmospheric stability on the fatigue life of wind turbines', *Jounal of Physics: Conference Series*, vol. 75, 2007. DOI: 10.1088/1742-6596/75/1/012056.

[43] A. Sathe, J. Mann, T. Barlas, W. Bierbooms and G. van Bussel, 'Atmospheric stability and its influence on wind turbine loads', English, in *Proceedings of Torque 2012, the science of making torque from wind*, The science of Making Torque from Wind 2012 : 4th scientific conference ; Conference date: 09-10-2012 Through 11-10-2012, 2012. [Online]. Available: http://www.forwind.de/makingtorque/Home.html.

[44] Kotur D., 'Individual pitch control for wind turbine load reduction recognizing atmospheric stability', 2012. [Online]. Available: https://windeurope.org/summit2016/conference/allfiles2/343_WindEurope2016presentation.pdf.

[45] S. Emeis and M. Turk, 'Comparison of logarithmic wind profiles and power law wind profiles and their applicability for offshore wind profiles', 2017.

[46] R. J. Barthelmie, J. Badger, S. C. Pryor, C. B. Hasager, M. B. Christiansen and B. H. Jørgensen, 'Offshore coastal wind speed gradients: Issues for the design and development of large offshore windfarms', *Wind Engineering*, vol. 31, no. 6, pp. 369–382, 2007. DOI: 10.1260/030952407784079762.

[47] R. B. Stull, *An Introduction to Boundary Layer Meteorology*, second. Springer Netherlands, 1988, ISBN: 978-94-009-3027-8. DOI: 10.1007/978-94-009-3027-8.

[48] J. Wu, 'Wind-stress coefficients over sea surface near neutral conditions—a revisit', *Journal of Physical Oceanography*, vol. 10, pp. 727–740, 5 1980.

[49] W. K. George and K. William, *Lectures in Turbulence for the 21st Century*. 2013.

[50] N. Carpmann, 'Turbulence intensity in complex environments and its influence on small wind turbines', 2011.

[51] Y. Hao, 'Wind farm wake modeling and analysis of wake impacts in a wind farm', 2016.

[52] J. Mann, 'The spatial structure of neutral atmospheric surface-layer turbulence', *Journal of Fluid Mechanics*, vol. 273, pp. 141–168, 1994.

[53] J Mann, 'Wind field simulation', English, *Probabilistic Engineering Mechanics*, vol. 13, pp. 269–282, 1998, ISSN: 0266-8920.

[54] v. T. Kármán, 'Progress in the statistical theory of turbulence', vol. 34, no. 11, pp. 530–539, 1948. DOI: 10.1073/pnas.34.11.530.

[55] N. Moskalenko, K. Rudion and O. Antje, 'Study of wake effects for offshore wind farm planning', Oct. 2010, pp. 1 –7.

[56] R. J. Barthelmie, K. Hansen, S. T. Frandsen, O. Rathmann, J. G. Schepers, W. Schlez, J. Philips, Rados, A. Zervos, E. S. Politis and P. K Chaviaropoulos, 'Modelling and measuring flow and wind turbine wakes in large wind farms offshore', 2009. DOI: 10.1002/we.348.

[57] W. J. Eecen P. J. and E. Bot, 'Offshore wind farms: Losses and turbulence in wakes, Modeling and validation', 2011.

[58] A Crespo, Hernández and J. Frandsen, 'Survey of modelling methods for wind turbine wakes and wind farms', 1999.

[59] C. B. Hasager, 'Using satellite sar to characterize the wind flow around offshore wind farms', 2003, ISSN: 1996-1073.

[60] N. G. Nygaard, 'Wakes in very large wind farms and the effect of neighbouring wind farms', *Journal of Physics: Conference Series*, vol. 524, no. 6, 2014. DOI: 10.1088/1742-6596/524/1/012162.

[61] G. España, S. Aubrun, S. Loyer and P. Devinant, 'Spatial study of the wake meandering using modelled wind turbines in a wind tunnel', *Wind energy*, vol. 14, pp. 923–937, 2011. DOI: 10.1002/we.515.

[62] R.-E. Keck, R. Mikkelsen, N. Troldborg, M. de Maré and K. S. Hansen, 'Synthetic atmospheric turbulence and wind shear in large eddy simulations of wind turbine wake', *Wind energy*, vol. 17, no. 8, 2014. DOI: 10.1002/we.1631.

[63] L. V. Davide Trabucchi and M. Kühn, '3-d shear-layer model for the simulation of multiple wind turbine wakes: Description and first assessment', 2017.

[64] C. Hasager, A. Rasmussen L.and Peña and P.-E Jensen L.E.; Réthoré, 'Wind farm wake: The horns rev photo case', *Energies*, vol. 6, no. 2, pp. 696–716, 2013. DOI: 10.3390/en6020696.

[65] S. Frandsen, 'Turbulence and turbulence-generated structural loading in wind turbine clusters', English, Risø-R-1188(EN), PhD thesis, 2007, ISBN: 87-550-3458-6.

[66] M. C. Brower and M. R. Nicholas, 'The openwind deep-array wake model, Development and validation', 2011.

[67] G. Larsen, H. Madsen Aagaard, F. Bingöl, J. Mann, S. Ott, J. Sørensen, V. Okulov, N. Troldborg, N. Nielsen, K. Thomsen, T. Larsen and R. Mikkelsen, *Dynamic wake meandering modeling*, English, ser. Denmark. Forskningscenter Risoe. Risoe-R 1607(EN). Risø National Laboratory, 2007, ISBN: 978-87-550-3602-4.

[68] B Lange, H. Waldl, A. G. Guerrero and D. Heinemann, 'Modelling of offshore wind turbine wakes with the wind farm program flap', vol. 6, 2003, 87–104. DOI: 10.1002/we.84.

[69] H.-P. Waldl, 'Modellierung der leistungsabgabe von windparks und optimierung der aufstellungsgeometrie', German, PhD thesis, University of Oldenburg, Department of Physics, 1997.

[70] E. Maguire, 'Lillgrund', [Online]. Available: https://windbench.net/lillgrund.

[71] T. Gögmen and G. Giebel, 'Estimation of turbulence intensity using rotor effective wind speed in lillgrund and horns rev-i offshore wind farms', English, *Renewable Energy*, vol. 99, pp. 524–532, 2016, ISSN: 0960-1481. DOI: 10.1016/j.renene.2016.07.038.

[72] E. Machefaux, G. Larsen and J. Murcia Leon, 'Engineering models for merging wakes in wind farm optimization applications', English, vol. 625, IOP Publishing, 2015. DOI: 10.1088/1742-6596/625/1/012037.

[73] T. Larsen, G. Larsen, H. Aagaard Madsen and S. Petersen, 'Wake effects above rated wind speed. an overlooked contributor to high loads in wind farms', English, in *Scientific Proceedings. EWEA Annual Conference and Exhibition 2015*, European Wind Energy Association (EWEA), 2015, pp. 95–99, ISBN: 9782930670003.

[74] H. Aagaard Madsen, T. Larsen, G. Larsen and K. Hansen, 'Wake flow characteristics at high wind speed', English, in *Proceedings of the 34th Wind Energy Symposium*, American Institute of Aeronautics and Astronautics, 2016. DOI: 10.2514/6.2016-1522.

[75] I. Katic, J. Højstrup and N. Jensen, 'A simple model for cluster efficiency', English, in *EWEC'86. Proceedings. Vol. 1*, W. Palz and E. Sesto, Eds., A. Raguzzi, 1987, pp. 407–410.

[76] H. Aagaard Madsen, T. Larsen, G. Larsen and K. Hansen, 'Wake flow characteristics at high wind speed', English, in *Proceedings of the 34th Wind Energy Symposium*, American Institute of Aeronautics and Astronautics, 2016. DOI: 10.2514/6.2016-1522.

[77] H. Zong and F. Porté-Agel, 'A momentum-conserving wake superposition method for wind farm power prediction', *Journal of Fluid Mechanics*, vol. 889, 2020. DOI: 10.1017/jfm.2020.77.

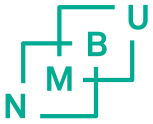

Norges miljø- og biovitenskapelige universitet
Noregs miljø- og biovitskapelege universitet
Norwegian University of Life Sciences

Postboks 5003
NO-1432 Ås
Norway